Multimedia Tools and Applications (2021) 80:35543–35583
https://doi.org/10.1007/s11042-020-10467-7

1166: ADVANCES OF MACHINE LEARNING IN DATA ANALYTICS AND VISUAL INFORMATION PROCESSING

A leader Harris hawks optimization for 2-D Masi entropy-based multilevel image thresholding

Manoj Kumar Naik[1] · **Rutuparna Panda**[2] · **Aneesh Wunnava**[1] · **Bibekananda Jena**[3] · **Ajith Abraham**[4]

Received: 8 March 2020 / Revised: 18 October 2020 / Accepted: 29 December 2020 /
Published online: 6 February 2021

Abstract

The multilevel image thresholding is one of the important steps in multimedia tools to understand and interpret the object in the real world. Nevertheless, 1-D Masi entropy is quite new in the thresholding application. However, the 1-D Masi entropy-based image thresholding fails to consider the contextual information. To address this problem, we propose a 2-D Masi entropy-based multilevel image thresholding by utilizing a 2-D histogram, which ensures the contextual information during the thresholding process. The computational complexity in multilevel thresholding increases due to the exhaustive search process, which can be reduced by a nature-inspired optimizer. In this work, we propose a leader Harris hawks optimization (LHHO) for multilevel image thresholding, to enhance the exploration capability of Harris hawks optimization (HHO). The increased exploration can be achieved by an adaptive perching during the exploration phase together with a leader-based mutation-selection during each generation of Harris hawks. The performance of LHHO is evaluated using the standard classical 23 benchmark functions and found better than HHO. The LHHO is employed to obtain optimal threshold values using 2-D Masi entropy-based multilevel thresholding objective function. For the experiments, 500 images from the Berkeley segmentation dataset (BSDS 500) are considered. A comparative study on state-of-the-art algorithm-based thresholding methods, using segmentation metrics such as – peak signal-to-noise ratio (PSNR), structural similarity index (SSIM), and the feature similarity index (FSIM), is performed. The experimental results reveal a remarkable difference in the thresholding performance. For instance, the average *PSNR* values (computed over 500 images) for the level 5 are increased by 2% to 4% in case of 2-D Masi entropy over 1-D Masi entropy.

Keywords Swarm intelligence · Harris hawks optimization · Optimal multilevel image thresholding · Multimedia applications · Masi entropy

✉ Manoj Kumar Naik
naik.manoj.kumar@gmail.com

Extended author information available on the last page of the article

1 Introduction

Image segmentation is an important step in image processing, in which one can extract a set of meaningful homogeneous sub-regions [4]. The thresholding is one of the most popular approaches in image segmentation. The thresholding is generally founded on the similarity approach based on the pixel intensity and the corresponding histogram of an image. Several global thresholding methods are presented in the literature [13, 14, 45, 55, 56, 59, 74, 76] to segment the image, extract the patterns of interest. The thresholding is broadly classified into a bi-level and a multilevel approach. The bi-level thresholding partitions the image into two different sub-regions, whereas the multilevel image thresholding is an extension of the bi-level thresholding, in which the image is partitioned into more than two different sub-regions. As the bi-level thresholding does not provide us the desired pattern for real-life problems, the multilevel image thresholding is strongly recommended [7].

The histogram-based approach is more popular in thresholding-based image segmentation [55, 59], in which we simply need to determine the threshold (intensity) value that helps to partition the image into different subregions. Some valuable works found in the literature for the one-dimensional histogram-based thresholding approach are – Otsu's method [43], Kapur's entropy [25], Tsallis entropy [48, 50, 64, 65], Rènyi entropy [52], and Masi entropy [35]. To improve the segmentation performance, some researchers extended the one-dimensional histogram-based thresholding problem to a two-dimensional histogram-based thresholding problem such as 2-D Otsu's method [33], 2-D Tsallis entropy [57], 2-D Renyi's entropy [53], 2-D Tsallis–Havrda–Charvát entropy [54], edge magnitude [46], and gray gradient [47]. As the number of threshold increases in multilevel image thresholding, the complexity of the problem increases. To overcome the time complexity, some researchers suggested recursive algorithms [32, 49, 73] with the help of lookup tables. However, the computational time increases [62] as the number of threshold increases.

The time complexity in multilevel image thresholding can be resolved using a soft computing approach. In this framework, several methods are discussed in the literature, most of the popular techniques are based on nature-inspired algorithms. The genetic algorithm (GA) was used for optimal threshold values using a reduced length of histogram based on wavelet transform in [18]. The Cuckoo search (CS) is used to obtain the multilevel threshold value by Tsallis entropy [1], Kapur's entropy [8], and edge magnitude [46] creation and shows an improvement of fitness value along with reduced computational time complexity. The artificial bee colony (ABC) was employed to reduce the computational time complexity to obtain the optimal multilevel threshold using maximizing the Kapur's entropy in [21] and Tsallis entropy in [75]. The make computational efficient the minimum cross entropy-based multilevel image thresholding approach over exhaustive search method is demonstrated using particle swarm optimization (PSO) in [72], honey bee mating optimization (HBMO) in [20], and firefly algorithm (FA) in [22]. The differential evolution (DE) was employed in 2-D Tsallis entropy in [57] to obtain the optimal threshold value and shown more effective as compared to PSO, GA, ABC based approach. Ant colony optimization (ACO) was employed as an optimization problem in Otsu's method in [78], which showed superior results over exhaustive Otsu's method in quality of solution and processing time. The whale optimization algorithm (WOA) and moth-flame optimization (MFO) is used in [12] to obtain the optimal threshold value using Otsu's method and found MFO shown better than WOA. The wind driven optimization (WDO) is used to obtain the multilevel threshold using maximizing the Kapur's entropy in [8]. The gray wolf optimizer (GWO) shown stability to obtain the optimal threshold value using Otsu's and Kapur's entropy method in [26] when compared with PSO and bacteria foraging optimization (BFO). The crow search algorithm (CSA) is employed to obtain the optimal threshold value using maximizing the Otsu's between class variance method in [11] and Kapur's entropy method in [66]. The krill herd optimization (KHO) [5] shows its superiority to obtain the optimal threshold values as compared to BFO, PSO, GA, and MFO (using both Otsu's and Kapur's entropy-based multilevel image thresholding). The coral reef optimization (CRO) is employed in diagonal cross entropy (DCE) in [2] to obtain the optimal threshold value by preserving the edge information in the image. The Masi entropy-based multilevel image thresholding approach using the water cycle algorithm (WCA) was developed in [24], which demonstrates its superiority in quality and convergence rate when compared with Tsallis entropy.

The basic or original version of the optimization algorithm cannot be used for all types of problems. So, the researcher hybridizes or modified the basic version of the optimization algorithm to improve the performance and utilize them in the various specific optimization problem. An adaptive crossover bacterial foraging optimization algorithm (ACBFOA) [39] was proposed by combining the crossover mechanism of GA in the bacteria foraging optimization algorithm (BFOA) to enhance the searching optimal solution and then apply it to face recognition problem. A hybrid Cuckoo search-gravitational search algorithm (CS-GSA) was proposed in [40] to increase the exploration capability of CS using the gravitational search algorithm (GSA) parameter and then apply it to recursive filter design an signal processing application. A dividing-based many-objective evolutionary algorithm for large-scale feature selection (DMEA-FS) [28] was developed in the framework of many-objective evolutionary algorithm (MaOEO) for feature selection. A whale optimization algorithm – differential evolution (WOA-DE) is proposed in [31] by replacing the exploration phase of WOA using crossover and mutation operator of DE for better efficiency in 3D mesh modeling. A multi objective sparse span array (MOSSA) algorithm is proposed in [29] based on the framework of multi objective particle swarm optimization (MOPSO) for better antenna design. The Biogeography-based Optimization algorithm with Elite Learning (BBO-EL) is proposed in [9] by incorporating the elite learning operator based on PSO and successfully applied in multimodal medical image registration.

Some of the advancements in this framework and application to multilevel image thresholding are discussed here. The comparative quantum particle swarm optimization (CQPSO) is proposed in [17] to enhance the convergence rate and conquer the dimensionality problem and employed to obtain the optimal threshold efficiently using Otsu's method. A modification of swarming and the reproduction behavior of BFOA leads to a modified bacterial foraging algorithm (MBFO) [58], which shows better performance than BFOA, PSO, and GA based approach for multilevel image thresholding using Kapur's entropy. The FA utilizes the Brownian distribution in the Brownian distribution guided firefly algorithm (BDFA) is employed to obtain the optimal threshold value based on the Otsu's method and shows better performance over FA in [63]. A hybridization of CS reset strategy in DE exhibits on hybrid differential evolution (HjDE) [38] and utilize in Otsu's method based multilevel image thresholding to obtain threshold. A hybrid optimization algorithm bird mating optimization–differential evolution (BMO-DE) [3] by integrating DE in bird mating optimization (BMO) to increase the efficiency of Kapur's entropy and Otsu's method based multilevel image thresholding. To increase the efficiency of the Tsallis entropy in multilevel image thresholding an improved thermal exchange optimization is employed [67], which shows better performance than CSA, PSO, flower pollination algorithm (FPA), and bat algorithm (BA/BAT). Multi-objective differential evolution and firework algorithm for automatic simultaneous clustering and classification algorithm (MASCC-DE/FWA) [30] is developed by hybridizing the search strategy of DE and firework algorithm (FWA) to demonstrate the advantage of classification problem in image segmentation. This has motivated the authors to investigate a new multilevel image thresholding approach to enrich the image segmentation techniques as an important component of multimedia tools and applications.

The focus of the work is to develop a 2-D Masi entropy-based multilevel image thresholding to overcome the disadvantage of 1-D Masi entropy. The 1-D Masi entropy was successfully applied in bi-level thresholding in [42], and further extended to multilevel image thresholding in [23, 24, 27, 60]. As the 1-D Masi entropy depends on the image histogram that is formed in the knowledge of the occurrence of gray level information in the image. So the 1-D histogram suffers from the lack of contextual information, because it doesn't consider the spatial correlation between pixels [20], which can be overcome by a 2-D histogram. This led us to extend the 1-D Masi entropy idea to the 2-D Masi entropy in multilevel image thresholding, which uses the 2-D histogram to obtain the Masi entropy. The 2-D Masi entropy-based multilevel image thresholding is an exhaustive search process of $O(L^{2K})$ for K threshold in a L gray level image, which is quite expensive [62] . This led us to focus on another development, to find an efficient optimizer as the multilevel image thresholding problem can be considered as a specific optimization problem. For this purpose, we have chosen a new metaheuristic algorithm Harris hawks optimization (HHO) proposed in [19]. The HHO is inspired by the cooperative perching strategy of Harris hawks. The HHO has quite impressive results when compared with some well-known optimization algorithms – GA [61], PSO [61], biogeography-based optimization (BBO) [61], FPA [69], GWO [37], BA/BAT [70], FA [15], CS [16], MFO [36], teaching-learning-based optimization (TLBO) [51] and DE [61] described in [19].

However, the exploration behavior of Harris hawks depends on the equal perching chance (a probability of 0.5). Therefore, its exploration is limited and random. This has motivated us to use an adaptive perch probability decided by the fitness of the Harris hawks in an exploration stage. The second disadvantage in HHO is that in the mid of the search process the escape energy is limited within unity, which again limits the exploration. The second disadvantage is overcome by a leader-based mutation-selection approach. This leads us to propose a leader Harris hawks optimization (LHHO) based on the simultaneous mutation and crossover using the three best leader Harris hawks along with an adaptive perch probability to enhance the exploration. The LHHO inherently includes these two new ideas. The performance of the newly coined LHHO is evaluated using twenty-three well known classical unimodal and multimodal benchmark test functions [39, 41, 71], which shows significant improvement over the HHO due to enhanced exploration. This encourages us to employ the LHHO to find the optimal threshold values using the 2-D Masi entropy. To visualize the performance of our proposed 2-D Masi entropy, the results are compared with 1-D Masi entropy. For the experiment, 500 images from the Berkeley Segmentation Data Set (BSDS 500) [34] are considered. The segmented image obtained using optimal threshold value is evaluated using the well-known quantitative metric such as peak signal-to-noise ratio (PSNR) [1], feature similarity (FSIM) [77], and structure similarity (SSIM) [79]. For the comparison of the LHHO based multilevel image thresholding, other state-of-the-art optimization algorithm based methods such as – CS [1], PSO [72], FA [22], WDO [8], Sooty tern optimization algorithm (STOA) [10], DE [57] are used including the HHO [19].

The main contributions of this work are as follows:

- A leader Harris hawks optimization (LHHO) is proposed to enhance the exploration capability of the HHO by augmenting the adaptive perch probability and leader-based mutation-selection approach. The LHHO is evaluated on 23 well-known unimodal and multimodal benchmark functions, which shows significant improvement over the HHO.
- A 2-D Masi entropy-based multilevel image thresholding is suggested (extension of the 1-D Masi entropy) that uses a 2-D histogram considering the contextual information during the thresholding process.
- An LHHO based multilevel image thresholding is proposed based on 2-D Masi entropy, which is validated using the BSDS 500 dataset and various state-of-the-art optimization algorithms.

The rest of the paper is organized as follows. In Section 2, a brief review of 1-D Masi entropy and the HHO algorithm are discussed. The proposed leader Harris hawks optimisations (LHHO) and its performance of benchmark functions are presented in Section 3. The 2-D Masi entropy-based thresholding approach is described in Section 4. The performance of the evolutionary 2-D Masi entropy-based multilevel image thresholding using the LHHO is presented in Section 5. Finally, the concluding remarks are drawn in Section 6.

2 Preliminaries

2.1 1-D Masi entropy-based image thresholding

A generalized entropy was introduced by Masi in [35], which is successfully applied to a bi-level thresholding in [42] and multilevel image thresholding in [23, 24, 27, 60]. The Masi entropy can handle the additive and non-extensive information in the physical system. The thresholding selection of an image using Masi entropy mainly depends on the 1-D histogram.

Let us consider a gray level image I of dimension $M \times N$, which has L number of gray levels in the range of $[0, L-1]$. The pixel with the gray level values at spatial coordinate (x, y) is represented as $f(x, y)$, where $x \in [1, 2, \cdots, M]$, and $y \in [1, 2, \cdots, N]$. Let n_i represent the number of pixels with gray level value i, where $i \in [0, 1, \cdots, L-1]$. Then the probability of each gray level can be represented as

$$p_i = \frac{n_i}{M \times N}, i \in [0, 1, \cdots, L-1] \tag{1}$$

and it must satisfy

$$\sum_{i=0}^{L-1} p_i = 1, \text{where } p_i > 0. \tag{2}$$

The bi-level thresholding consists of two classes as foreground (C_f) and background (C_b), which is separated using a threshold value $t \in [1, 2, \cdots, L-2]$. Then the foreground class probability (ω_f) and background class probability (ω_b) are defined as

$$\omega_f = \sum_{i=0}^{t-1} p_i, \tag{3}$$

and

$$\omega_f = \sum_{i=t}^{L-1} p_i. \tag{4}$$

The foreground class Masi entropy (H_f) and background class Masi entropy (H_b) are calculated as

$$H_f = \frac{1}{1-r} \log\left[1-(1-r)\sum_{i=0}^{t-1}\left(\frac{p_i}{\omega_f}\right)\log\left(\frac{p_i}{\omega_f}\right)\right], \tag{5}$$

and

$$H_b = \frac{1}{1-r} \log\left[1-(1-r)\sum_{i=t}^{L-1}\left(\frac{p_i}{\omega_b}\right)\log\left(\frac{p_i}{\omega_b}\right)\right] \tag{6}$$

where r is the entropic parameter is set to 0.5.

The bi-level thresholding based on Masi entropy is described by

$$H_{(t)} = H_f + H_b, \tag{7}$$

and the optimal threshold t^* based on Masi entropy can be defined as

$$t^* = \text{argmax}_{0<t<L-1}\left(H_{(t)}\right). \tag{8}$$

The authors in [23, 24, 27, 60] extended the bi-level thresholding to multi-level thresholding using Masi entropy, where the number of thresholds is more than one. Let us consider that the image is divided into $K+1$ classes as $C = \{C_0, C_1, \cdots, C_{K-1}, C_K\}$ which is a set of the foreground class C_0, intermediate classes $C_{i=1,2,\cdots K-1}$, and the background class C_K based on the K threshold values $t_1, t_2, \cdots, t_K$. The gray level values of different classes are defined as:

$$\begin{gathered}[0, t_1-1]\in C_0 \\ [t_1, t_2-1]\in C_1 \\ \cdots \\ [t_K, L-1]\in C_K\end{gathered} \tag{9}$$

where $0 < t_1 < t_2 < \cdots < t_K < L-1$. So, let assign $t_0 = 0$ and $t_{K+1} = L$.

The different class probability for multilevel thresholds are defined as

$$\omega_0 = \sum_{i=0}^{t_1-1} p_i, \omega_1 = \sum_{i=t_1}^{t_2-1} p_i, \cdots, \omega_K = \sum_{i=t_K}^{L-1} p_i. \tag{10}$$

Then, the Masi entropy H_j for the ith class calculated as:

$$H_j = \frac{1}{1-r} \log\left[1-(1-r)\sum_{i=t_j}^{t_{j+1}-1}\left(\frac{p_i}{\omega_j}\right)\log\left(\frac{p_i}{\omega_j}\right)\right], \text{where } 0\le j\le K. \tag{11}$$

The multilevel image thresholding based on Masi entropy is described by

$$H_{(t_1,t_2,\cdots,t_K)} = H_0 + H_1 + \cdots + H_K \tag{12}$$

and the optimal threshold $\{t_1^*, t_2^*, \cdots, t_K^*\}$ based on Masi entropy can be defined as:

$$\{t_1^*, t_2^*, \cdots, t_K^*\} = \text{argmax}_{0<t_1<t_2<\cdots<t_K<L-1}\left(H_{(t_1,t_2,\cdots,t_K)}\right). \tag{13}$$

Finally, Eq. (13) is used as the fitness function to solve the problem of multilevel image thresholding in [23, 24, 27, 60]. However, different optimization techniques are suggested by these authors to maximize the objective function Eq. (13).

2.2 Harris hawks optimization (HHO)

In the year 2019, Harris hawks optimization (HHO), a population-based nature-inspired optimization algorithm is proposed in [19]. The HHO is inspired by the cooperative behavior and chasing style of the Harris Hawks to capture a prey called surprise pounce, which is also known as the "seven kills" strategy. Of the seven kills intelligent strategy, several hawks attack the prey cooperatively from different directions and converge on the detected prey. Sometimes, it also happens that some hawks suddenly move to another nearby place to find the new prey. Based on these behaviors of the Harris hawks, HHO is modeled with the exploration and the exploitation phases.

Let N population of hawks in search areas are cooperatively searching for the prey, then one can define $X_i(t)$ as the current position vector of hawks for i ($i = 1, 2, \cdots, N$), $X_{prey}(t)$ is the best position vector among all hawks in a search area or position vector of the prey for the current generation t ($0 < t \leq t_{max}$) in a maximum generation t_{max}.

2.2.1 Exploration phase

The Harris hawks perch randomly on some location and wait to detect the prey based on the equal chance q for every two different strategies. One strategy is based on the position of other family members when $q < 0.5$, in which they are close enough to attack the prey. The other strategy is when the Harris hawk perches in some tall tree and waiting for the prey with a chance of $q \geq 0.5$. These two strategies are modeled as:

$$X_i(t+1) = \begin{cases} X_{random}(t) - r_1 |X_{random}(t) - 2r_2 X_i(t)| & q \geq 0.5 \\ X_{prey}(t) - X_m(t) - r_3 (LB + r_4(UB - LB)) & q < 0.5 \end{cases} \tag{14}$$

where $X_i(t+1)$ is the next position vector of a hawk i ($i = 1, 2, \cdots, N$) in the generation $t + 1$, $X_{random}(t)$ is the position vector of a randomly selected hawk in the generation t, $X_m(t)$ is the mean position vector of all N hawks in the generation t and calculated as $X_m(t) = \frac{1}{N}\sum_{i=1}^{N} X_i(t)$, LB is the lower bound of the search space, UB is the upper bound of the search space; and $[r_1, r_2, r_3, r_4, q]$ are set of random numbers in the range (0, 1).

2.2.2 The transition between the exploration and the exploitation phase

The transition between the exploration and the exploitation depends on the escaping energy E of the prey in the range of (−2, 2), that can be modeled as:

$$E = 2E_0\left(1 - \frac{t}{t_{max}}\right) \tag{15}$$

where E_0 is the initial escaping energy of the prey in the range of (−1, 1) calculated as:

$$E_0 = 2 * rand(\cdot) - 1. \tag{16}$$

The initial escaping energy 0 to −1 represents the prey that is physically flagging and 0 to 1 represents that the prey is strengthening. When the escaping energy $|E| \geq 1$, the hawk tries to explore the prey location, and when $|E| < 1$, the hawk tries to exploit the nearby solutions.

2.2.3 Exploitation phase

The Harris hawks attack the intended prey, which is detected in the early phase by performing the surprise pounce in the exploitation phase. Let the prey always try to escape from the targeted area of hawks with an escaping chance r. When the escaping chance of $r < 0.5$, the prey successfully escapes, and for the escaping chance $r \geq 0.5$, the prey fails to escape before the surprise pounce performed by the hawk. Based on the escaping energy E of the prey, the hawk performs soft besiege (softly encircle the prey from various directions) when $|E| \geq 0.5$, and hard besiege (hardly encircle the prey from various directions) when $|E| < 0.5$. Based on the behavior of the prey, and the hawk chasing style, the HHO can be modeled using four possible attacking strategies as described below.

- *Soft besiege* ($r \geq 0.5$ and $|E| \geq 0.5$)

In this attacking strategy, the prey cannot escape, although it has enough energy to escape. During this attacking strategy, the hawk i ($i = 1, 2, \cdots, N$) softly encircle the prey until the prey is exhausted to perform the surprise pounce, which can be modeled as:

$$X_i(t+1) = X_{prey}(t) - X_i(t) - E\left|JX_{prey}(t) - X_i(t)\right| \tag{17}$$

$$J = 2(1 - r_5) \tag{18}$$

where J represents the jump strength of the prey during the escaping from the hawk target area, r_5 is a random number in the range (0, 1).

- *Hard besiege* ($r \geq 0.5$ and $|E| < 0.5$)

In this attacking strategy, the prey cannot escape as it is already exhausted. During this attacking strategy, the hawk i ($i = 1, 2, \cdots, N$) hardly encircles the prey and perform the surprise pounce. Which can be modeled as:

$$X_i(t+1) = X_{prey}(t) - E\left|X_{prey}(\mathrm{t}) - X_i(t)\right| \tag{19}$$

- *Soft besiege with progressive rapid dives* ($r < 0.5$ and $|E| \geq 0.5$)

In this attacking strategy, the prey has enough energy to escape, and the hawk softly encircles the prey before a surprise pounce. The prey uses the levy flight (LV) [6, 68] movements to escape from the targeted area of the hawk.

Let the hawk i ($i = 1, 2, \cdots, N$) performs the soft besiege by evaluating the previous move and prey location as:

$$Y_i = X_{prey}(t) - E\left|JX_{prey}(t) - X_i(t)\right|. \tag{20}$$

Then, the hawk compares its current move with the previous move to find it worthy or not. If it was not a worthy move, the hawk performs irregular, abrupt, and rapid dives while approaching the prey, which can be modeled as:

$$Z_i = Y_i + S \times LF(D) \tag{21}$$

where S is a random vector of dimension $1 \times D$, D is the dimension of the problem and LF [6, 68] is the levy flight movements, which is calculated as:

$$LF(x) = 0.01 \times \frac{u \times \sigma}{|v|^{\frac{1}{\beta}}}, \sigma = \left(\frac{\Gamma(1+\beta) \times \sin\left(\frac{\pi\beta}{2}\right)}{\Gamma\left(\frac{1+\beta}{2}\right) \times \beta \times 2^{\left(\frac{\beta-1}{2}\right)}}\right)^{\frac{1}{\beta}} \tag{22}$$

where u and v are random variables in the range (0, 1), and β(=1.5) is a constant.

Then the hawk i ($i = 1, 2, \cdots, N$) positions are updated in the soft besiege with progressive rapid dives as:

$$X_i(t+1) = \begin{cases} Y_i & \text{if } f(Y_i) < f(X_i(t)) \\ Z_i & \text{if } f(Z_i) < f(X_i(t)) \end{cases}. \tag{23}$$

- *Hard besiege with progressive rapid dives* ($r < 0.5$ and $|E| < 0.5$)

In this attacking strategy, the prey has not enough energy to escape, and the hawk hardly besieges before the surprise pounce to catch the prey. This attacking strategy is pretty like soft besiege with progressive rapid dives, but in this, the hawk considers the other hawks' location for escaping prey. So, the update rule of position vector in this attacking strategy is given as

$$X_i(t+1) = \begin{cases} Y_i & \text{if } f(Y_i) < f(X_i(t)) \\ Z_i & \text{if } f(Z_i) < f(X_i(t)) \end{cases} \tag{24}$$

where

$$Y_i = X_{prey}(t) - E\left|JX_{prey}(t) - X_m(t)\right|, \text{where } X_m(t) = \frac{1}{N}\sum_{i=1}^{N} X_i(t) \tag{25}$$

$$Z_i = Y_i + S \times LF(D). \tag{26}$$

2.2.4 Pseudocode of HHO

In the beginning, let us identify the dimension of the problem as D, number of hawks employed in a search space as N, upper boundary and lower boundary of the search space as UB and LB, maximum iterations as t_{max}, and a fitness function as f of a given problem statement. Then initialize the position vector of ith hawk as $X_i(t=1) = \left(x_i^1, x_i^2, \cdots, x_i^D\right)$ for D dimension problem at generation $t = 1$.

while ($t < t_{max}$)
{
I. Evaluate the fitness function $f(X_i)$ for hawk i ($i = 1,2,\cdots,N$).
II. Find the best position vector based on the best fitness function and assigned the value to X_{prey}.
III. for (each hawk X_i) do
  A. Calculate initial escape energy E_0 using Eq. (16).
  B. Calculate the jump strength J using Eq. (18).
  C. Update the escape energy E using Eq. (15).
  D. if ($|E| \geq 1$)
      Update the position vector $X_i(t+1)$ using Eq. (14)
    if ($|E| < 1$)
      if ($r \geq 0.5$ and $|E| \geq 0.5$)
        Update the position vector $X_i(t+1)$ using Eq. (17)
      elseif ($r \geq 0.5$ and $|E| < 0.5$)
        Update the position vector $X_i(t+1)$ using Eq. (19)
      elseif ($r < 0.5$ and $|E| \geq 0.5$)
        Update the position vector $X_i(t+1)$ using Eq. (23)
      else ($r < 0.5$ and $|E| < 0.5$)
        Update the position vector $X_i(t+1)$ using Eq. (24)
IV. $t = t + 1$.
} return the best solution X_{prey}.

3 The proposed leader Harris hawks optimization (LHHO)

The motivation for the development of the leader Harris hawks optimization (LHHO) comes from the exploration behavior of the Harris hawk. The disadvantage of the HHO is its limited exploration. The reason is the perching strategy, which depends on equal chance q [19]. As described in the HHO algorithm [19], the hawks perch based on the position of other family members if $q < 0.5$, otherwise perch in a random tall tree if $q \geq 0.5$. This can be overcome with a perch probability of the individual hawk.

Exploration phase ($|E| \geq 1$): Let us define an adaptive perch probability (p^i_{ap}) of ith hawk, which depends on the fitness value of the current hawk with position vector X_i as $f(X_i)$ of ith hawk, fitness value of the best performing hawk with the position vector X_{prey} as $f(X_{prey})$ and fitness value of the worst-performing hawk with the position vector X_{worst} as $f(X_{worst})$. Then the adaptive perch probability (p^i_{ap}) can be modeled as

$$p^i_{ap} = \frac{|f(X_i) - f(X_{prey})|}{|f(X_{worst}) - f(X_{prey})|}, i = 1, 2, \cdots, N \tag{27}$$

Then the exploration phase can be modeled as

$$X_i(new) = \begin{cases} X_{rand}(t) - r_1 |X_{rand}(t) - 2r_2 X_i(t)| & q \geq p^i_{ap} \\ (X_{prey}(t) - X_m(t)) - r_3(LB + r_4(UB - LB)) & q < p^i_{ap} \end{cases} \tag{28}$$

where $X_m(t)$ is the mean position vector of the current population of N hawks.

Exploitation phase ($|E| < 1$): The exploitation phase can be modeled four possible attacking strategies as described below which are like the HHO [19].

- *Soft besiege* ($r \geq 0.5$ and $|E| \geq 0.5$)

$$X_i(new) = X_{prey}(t) - X_i(t) - E\left|JX_{prey}(t) - X_i(t)\right| \tag{29}$$

where J is the jump strength as of Eq. (18).

- *Hard besiege* ($r \geq 0.5$ and $|E| < 0.5$)

$$X_i(new) = X_{prey}(t) - E\left|X_{prey}(t) - X_i(t)\right| \tag{30}$$

- *Soft besiege with progressive rapid dives* ($r < 0.5$ and $|E| \geq 0.5$)

$$X_i(new) = \begin{cases} Y_i & \textit{if } f(Y_i) < f(X_i(t)) \\ Z_i & \textit{if } f(Z_i) < f(X_i(t)) \end{cases}. \tag{31}$$

The Y_i and Z_i can be calculated using Eq. (20) and Eq. (21), respectively.

- *Hard besiege with progressive rapid dives* ($r < 0.5$ and $|E| < 0.5$)

$$X_i(new) = \begin{cases} Y_i & \textit{if } f(Y_i) < f(X_i(t)) \\ Z_i & \textit{if } f(Z_i) < f(X_i(t)) \end{cases}. \tag{32}$$

The Y_i and Z_i can be calculated using Eq. (25) and Eq. (26), respectively.

The HHO algorithm transition of the exploration to/from exploitation depends on the escape energy of the prey. The time-dependent behavior of the escape energy is presented in Fig. 1. As we can observe that after the 50% of the maximum iterations, the escape energy $|E|$ is always below 1. This shows that the HHO algorithm only performs the exploitation after 50% of the maximum iteration. This shows that the exploration is restricted, as a result, the optimal value may fall to a local minimum. To supplement the HHO, a leader-based mutation-selection approach, that helps to explore until the end, is proposed.

Leader-based mutation-selection Let us define the best hawks position vector X^t_{best}, the second-best hawks' position vector X^t_{best-1} and the third-best hawks' vector X^t_{best-2} based on the fitness function value of the new position vector $X(new)$ among N individual hawks. Then the new mutation position vector $X_i(mut)$ for ith hawk can be defined as

$$\begin{aligned} X_i(mut) = X_i(new) + 2*\left(1 - \frac{t}{t_{max}}\right)*(2*rand-1)\left(2*X^t_{best} - \left(X^t_{best-1} + X^t_{best-2}\right)\right) \\ + (2*rand-1)\left(X^t_{best} - X_i(new)\right) \end{aligned} \tag{33}$$

where $rand$ is a random number in the range (0, 1).

Then the position vector for the next generation $X_i(t+1)$ can be obtained by the selection process described in the Eq. (34). Similarly, the X_{prey} is updated using the Eq. (35).

$$X_i(t+1) = \begin{cases} X_i(mut) & f(X_i(mut)) < f(X_i(new)) \\ X_i(new) & f(X_i(mut)) \geq f(X_i(new)) \end{cases} \tag{34}$$

$$X_{prey} = \begin{cases} X_i(mut) & f(X_i(mut)) < f\left(X_{prey}\right) \\ X_i(new) & f(X_i(new)) < f\left(X_{prey}\right) \end{cases} \tag{35}$$

3.1 Pseudocode of LHHO

In the beginning, assign the parameters N, D, UB, LB, t_{max}.

Initialization: Generate the random position vector $X_i(t=1) = (x_i^1, x_i^2, \cdots, x_i^D)$ for ith hawk in a D dimensional problem at iteration $t = 1$.

Begin:

I. Evaluate the fitness function $f(X_i)$ for hawks i $(i = 1,2,\cdots,N)$.

II. Label the best position vector as X_{prey} and worst position vector as X_{worst} among N hawks based on best and worst fitness value obtained from Step I.

III. While $(t < t_{max})$

  A. For (each hawk X_i) do

    a. Update the escape energy E using Eq. (15).

    b. Calculate the jump strength J using Eq. (18).

    c. Calculate adaptive perch probability p_{ap}^i using Eq. (27).

    d. if $(|E| \geq 1)$

      Update the position vector $X_i(new)$ using Eq. (28).

    if $(|E| < 1)$

      if $(r \geq 0.5$ and $|E| \geq 0.5)$

        Update the position vector $X_i(new)$ using Eq. (29)

      elseif $(r \geq 0.5$ and $|E| < 0.5)$

        Update the position vector $X_i(new)$ using Eq. (30)

      elseif $(r < 0.5$ and $|E| \geq 0.5)$

        Update the position vector $X_i(new)$ using Eq. (31)

      else $(r < 0.5$ and $|E| < 0.5)$

        Update the position vector $X_i(new)$ using Eq. (32)

  B. Evaluate the fitness function $f\left(X_i(new)\right)$ for hawks i $(i = 1,2,\cdots,N)$.

  C. Label the X_{best}^t, X_{best-1}^t and X_{best-2}^t based on the ranking of the top three fitness values obtained in Step B.

  D. for (each hawk $X_i(new)$) do

    a. Calculate the new mutation position vector $X_i(mut)$ using Eq. (33).

    b. Evaluate the fitness value $f\left(X_i(mut)\right)$ of a new mutation position vector $X_i(mut)$.

    c. Select the next generation position vector $X_i(t+1)$ using the Eq. (34).

    d. Update the best position vector as X_{prey} using the Eq. (35).

IV. $t = t + 1$.

} return the best solution X_{prey}.

End

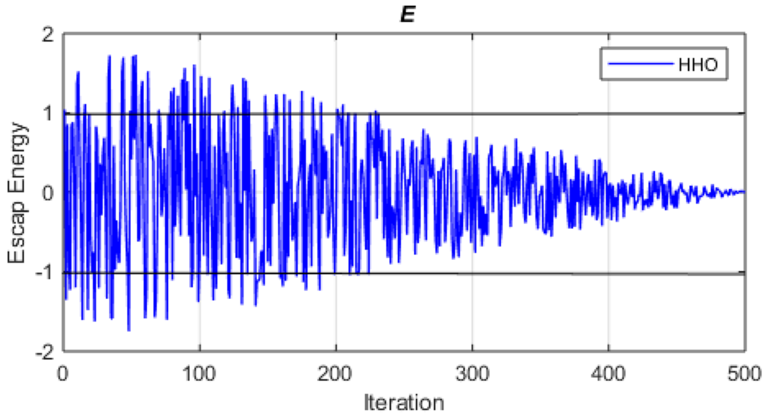

Fig. 1 Behavior of the escape energy of the prey in HHO during 500 iterations

3.2 Performance evaluation of LHHO

To examine the performance of the proposed LHHO, a comparison with the HHO [19] (with the help of 23 well-known test functions ($f_1 - f_{23}$) chosen from the literature [39, 41, 71]) is made. It is noteworthy to mention here that the test functions are divided in three groups as unimodal test functions ($f_1 - f_7$), multimodal test functions with varied dimension ($f_8 - f_{13}$) and multimodal test functions with fixed dimension ($f_{14} - f_{23}$), presented in Appendix 1. The unimodal test function has a unique optimal solution, and the convergence rate is more essential in the validation of an optimization algorithm. The multimodal test functions have many local minima, so avoidance of a local minimum is more concerned. Moreover, the performance at unimodal test function gives the exploitation capability, whereas the performance of multimodal test functions gives the exploration capability of the optimization algorithm.

The input parameters are chosen as $N = 20$, $t_{max} = 500$ and $\beta = 1.5$ for the performance evaluation of both the algorithms. Each algorithm runs 100 times to get the best optimal value '**Best**', worst optimal value '**Worst**', average optimal value '**Avg**', the standard deviation '**Std**', and the average time '**AvgTime**' in seconds. The best values are represented in boldface.

The statistical results of unimodal test functions ($f_1 - f_7$) and multimodal test functions with varied dimension ($f_8 - f_{13}$) for dimension $D = 30,100$ are presented in Table 1 and Table 2, respectively. All the unimodal test functions have shown significant improvement in the LHHO as compared to the HHO for all the statistical parameters, which is explicit from Tables 1 and 2. The convergence curve of three unimodal test functions is shown in Fig. 2. In the multimodal test functions with varied dimension, $f_{8,12,13}$ show the improvement while $f_{9,10,11}$ produce the same result (both in the LHHO and the HHO). From the convergence curve for three multimodal test functions, as shown in Fig. 3, it is observed that the convergence of the LHHO is faster than the HHO concerning iterations. The convergence curves implicitly suggest that the LHHO is useful for function optimization.

The statistical results of multimodal test functions with fixed dimension ($f_{14} - f_{23}$) are presented in Table 3 and the sample convergence curves are presented in Fig. 4. From a comparison (see Table 3), it is seen that the statistical parameter '*Best*' performs in the same way in both the LHHO and HHO. However, the statistical parameters '*Avg*', '*Worst*', and '*Std*' of the LHHO show their superiority over the HHO. To be precise, the overall statistical performance of the LHHO is better than the HHO. The LHHO takes 35% more time as compared to the HHO (for 500 iterations), which may be treated as a penalty to obtain better optimal solutions. However, the convergence is faster in the case of LHHO, because it takes less number of iterations than HHO. Finally, the LHHO shows better results/convergence as compared to the HHO due to the adaptive perching strategy and the leader-based mutation-selection approach to enhance the exploration, keeping unchanged the exploitation ability of the HHO. Interestingly, these two newly investigated features ensure better exploration by the LHHO.

4 The proposed 2-D Masi entropy-based multilevel image thresholding

In this section, we extend the idea of the 1-D Masi entropy [23, 24, 27, 60] to introduce a new 2-D Masi entropy-based multilevel image thresholding technique by utilizing the basic principle as described in Section 2.1 and the idea of 2-D histogram discussed in [44].

Here, we suggest an extension of the 1-D histogram of an image I of size $M \times N$ into a 2-D histogram. The local average $g(x, y)$ of the gray level values of an image $f(x, y)$ for a window of size $w \times w$ is formulated as:

$$g(x,y) = \left\lfloor \frac{1}{w \times w} \sum_{m=-l}^{l} \sum_{n=-l}^{l} f(x+m, y+n) \right\rfloor \tag{36}$$

Note that $w < \min(M, N)$ and $\left\lfloor \frac{w}{2} \right\rfloor$ represents the integer part only.

The gray level values of the image $f(x, y)$, and the local average $g(x, y)$ of the gray level values are used to construct the 2-D histogram using the co-occurrences (n_{ij}).

$$n_{ij} = probe(f(x,y) = i \; and \; g(x,y) = j) \tag{37}$$

Then the normalized 2-D histogram (p_{ij}) of the index (i, j) is approximated as:

$$p_{ij} = \frac{n_{ij}}{M \times N} \tag{38}$$

where $M \times N$ represent the image size. A pictorial representation of a 2-D histogram is presented in Fig. 5, which covers a square region of size $L \times L$.

The bi-level thresholding divides the image into two classes; known as the foreground class (C_f) and the background class (C_b) (using the threshold point (s, t)). The s is the local average threshold and t is the gray level threshold. The 2-D histogram plane for the bi-level thresholding is shown in Fig. 5a, in which the main interest areas useful for thresholding are 1st and 4th quadrants, as they represent the foreground and the background class information. The 2nd and 3rd quadrants generally contain edge and noise information only. The probability distribution of the foreground class φ_f and the background class φ_b is given as:

$$\varphi_f(s,t) = \sum_{i=0}^{s-1} \sum_{j=0}^{t-1} p_{ij} \tag{39}$$

Table 1 Statistical result of unimodal test functions f_{1-7}

Function	Statistical Parameter	D=30		D=100	
		LHHO	HHO	LHHO	HHO
f_1	Best	**1.5980E-163**	7.2234E-111	**5.5624E-158**	3.3807E-111
	Avg	**2.4662E-133**	1.7364E-88	**6.1080E-135**	2.9372E-88
	Worst	**1.2326E-131**	8.3354E-87	**3.0417E-133**	1.0732E-89
	Std	**1.7432E-132**	1.1788E-87	**4.3013E-134**	5.0777E-89
	AvgTime (in a sec)	0.185	**0.148**	0.254	0.201
f_2	Best	**7.3454E-84**	6.0855E-57	**3.7036E-81**	4.6870E-58
	Avg	**1.1200E−67**	2.7046E-47	**2.0113E-70**	5.3235E-46
	Worst	**5.5640E-66**	1.2113E-45	**4.0186E-69**	1.1850E-47
	Std	**7.8677E-67**	1.7181E-46	**7.9243E-70**	7.5245E-47
	AvgTime (in a sec)	0.181	**0.146**	0.251	0.202
f_3	Best	**1.8615E−133**	3.8435E-96	**1.9997E-122**	6.8118E-92
	Avg	**3.0938E-89**	2.2787E-62	**2.9643E-58**	1.7817E-47
	Worst	**6.7022E-88**	1.1381E-60	**1.4801E-56**	8.9083E-46
	Std	**1.3136E-88**	1.6095E-61	**2.0931E-57**	1.2598E-46
	AvgTime (in a sec)	0.833	**0.595**	2.816	1.964
f_4	Best	**3.8206E-80**	4.0495E-57	**1.9349E-82**	6.3618E-61
	Avg	**2.8928E-67**	4.9806E-46	**9.2692E-65**	1.2253E-44
	Worst	**1.4389E-65**	2.4631E-44	**3.0505E-63**	5.7794E-43
	Std	**2.0347E-66**	3.4827E-45	**4.8138E-64**	8.1747E-44
	AvgTime (in a sec)	0.213	**0.177**	0.314	0.243
f_5	Best	**1.0704E-05**	7.9565E-05	**5.0781E-07**	2.2986E-04
	Avg	**0.0018**	0.0223	**0.0068**	0.0943
	Worst	**0.0137**	0.1838	**0.0607**	0.5098
	Std	**0.0025**	0.0353	**0.0112**	0.1155
	AvgTime (in a sec)	0.325	**0.255**	0.456	0.372
f_6	Best	**2.2306E-11**	3.4489E-06	**1.2148E-07**	3.7174E-06
	Avg	**2.4262E-05**	2.8751E-04	**6.4516E-05**	0.0011
	Worst	**3.0985E-04**	0.0021	**8.5748E-04**	0.0042
	Std	**5.2553E-05**	4.0999E-04	**1.5705E-04**	0.0012
	AvgTime (in a sec)	0.236	**0.194**	0.386	0.304
f_7	Best	3.3390E-06	**2.7164E-06**	7.8745E-06	**2.7784E-06**
	Avg	**1.6445E-04**	2.7837E-04	**1.6590E-04**	2.0549E-04
	Worst	**8.8218E-04**	0.0014	**7.3319E-04**	8.6514E-04
	Std	**1.6772E-04**	2.9431E-04	**1.4626E-04**	2.0845E-04
	AvgTime (in a sec)	0.524	**0.397**	1.295	0.935

$$\varphi_b(s,t) = \sum_{i=s}^{L-1}\sum_{j=t}^{L-1} p_{ij} \tag{40}$$

where $i, j = 0, 1, \cdots, L-1$. Note that the contribution of 2nd and 3rd quadrants are negligible. Hence, $\varphi_b(s, t) \approx 1 - \varphi_f(s, t)$ *.

The 2-D Masi entropy of the foreground class ($H_f(s, t)$) and the background class ($H_b(s, t)$) are formulated as

$$H_f(s,t) = \frac{1}{1-r}\log\left[1-(1-r)\sum_{i=0}^{s-1}\sum_{j=0}^{t-1}\left(\frac{p_{ij}}{\varphi_f(s,t)}\right)\log\left(\frac{p_{ij}}{\varphi_f(s,t)}\right)\right], \tag{41}$$

Table 2 Statistical result of multimodal test functions with varied dimension f_{8-13}

Function	Statistical Parameter	D=30		D=100	
		LHHO	HHO	LHHO	HHO
f_8	Best	-6.1288E+05	**-1.2569E+04**	−2.0128E+06	**−4.1898E+04**
	Avg	−3.2593E+05	**−1.2503E+04**	−1.1637E+06	**−4.1722E+04**
	Worst	−2.7315E+04	**−9.5072E+03**	−1.9142E+03	**−3.3619E+04**
	Std	1.7167E+05	**433.4012**	4.9063E+05	**1.1698E+03**
	AvgTime (in a sec)	0.307	0.277	0.514	0.459
f_9	Best	**0**	**0**	**0**	**0**
	Avg	**0**	**0**	**0**	**0**
	Worst	**0**	**0**	**0**	**0**
	Std	**0**	**0**	**0**	**0**
	AvgTime (in a sec)	0.318	0.245	0.453	0.392
f_{10}	Best	**8.8816E-16**	**8.8816E-16**	**8.8816E-16**	**8.8816E-16**
	Avg	**8.8816E-16**	**8.8816E-16**	**8.8816E-16**	**8.8816E-16**
	Worst	**8.8816E-16**	**8.8816E-16**	**8.8816E-16**	**8.8816E-16**
	Std	**0**	**0**	**0**	**0**
	AvgTime (in a sec)	0.282	0.236	0.446	0.385
f_{11}	Best	**0**	**0**	**0**	**0**
	Avg	**0**	**0**	**0**	**0**
	Worst	**0**	**0**	**0**	**0**
	Std	**0**	**0**	**0**	**0**
	AvgTime (in a sec)	0.346	0.279	0.600	0.456
f_{12}	Best	**1.4828E-09**	4.9614E-08	**4.1649E-10**	8.5261E-09
	Avg	**1.5556E-06**	2.4479E-05	**5.8844E-07**	9.1718E-06
	Worst	**1.4832E-05**	2.0284E-04	**7.3986E-06**	7.3270E-05
	Std	**2.6323E-06**	3.6282E-05	**1.1981E-06**	1.4833E-05
	AvgTime (in a sec)	1.251	0.915	3.136	2.211
f_{13}	Best	**9.4345E-08**	2.8557E-08	**1.7494E-08**	1.8144E-07
	Avg	**1.5248E-05**	2.9853E-04	**5.4173E-05**	5.4056E-04
	Worst	**6.2588E-05**	0.0021	**5.2259E-04**	0.0037
	Std	**1.8103E-05**	4.0745E-04	**1.1093E-04**	8.1821E-04
	AvgTime (in a sec)	1.245	0.894	3.078	2.200

and

$$H_b(s,t) = \frac{1}{1-r}\log\left[1-(1-r)\sum_{i=s}^{L-1}\sum_{j=t}^{L-1}\left(\frac{p_{ij}}{\varphi_b(s,t)}\right)\log\left(\frac{p_{ij}}{\varphi_b(s,t)}\right)\right] \tag{42}$$

where r is the entropic parameter set to 0.5.

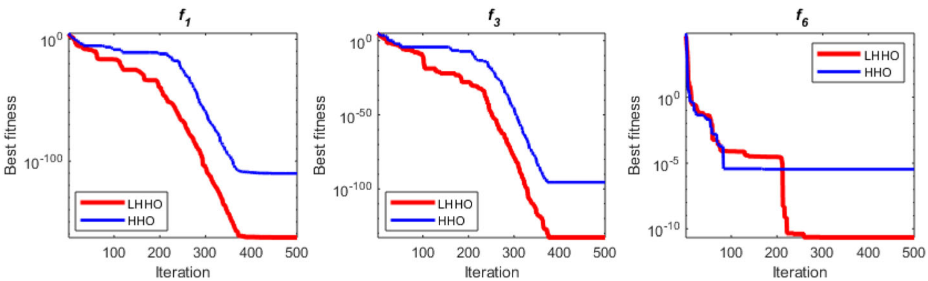

Fig. 2 Convergence curve of three unimodal test functions with $D = 30$

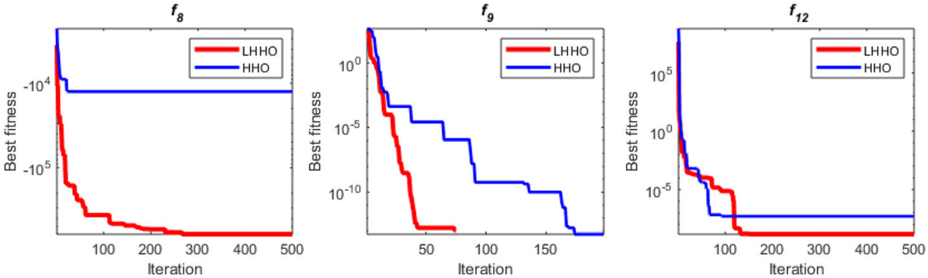

Fig. 3 Convergence curve of three multimodal test functions with the varied dimension with $D = 30$

The optimal threshold $\{s^*, t^*\}$ for 2-D Masi entropy based bi-level thresholding can be formulated as a maximization criterion given as:

$$\{s^*, t^*\} = \operatorname{argmax}\left[H_f(s,t) + H_b(s,t)\right] \tag{43}$$

subject to the conditions $0 < s < L - 1$, and $0 < t < L-1$.

The multilevel image thresholding using the 2-D histogram for K threshold coordinates $[s_1t_1, s_2t_2, \cdots, s_Kt_K]$ [47, 57] are discussed here. The K threshold points separate the image into a set of $K + 1$ classes as $C = \{C_0, C_1, \cdots, C_{K-1}, C_K\}$. The 2-D histogram plane of the multilevel thresholding for $K + 1$ classes is shown in Fig. 5b, in which the diagonal quadrants are of the main interest for thresholding. The other quadrants are ignored as they consist of edge and noise components. The probability distribution of different $K + 1$ classes is expressed as:

Table 3 Statistical result of multimodal test functions with fixed dimension f_{14-23}

Function	Algorithm	Statistical Parameter				
		Best	Avg	Worst	Std	AvgTime (in a sec)
f_{14}	LHHO	**0.9980**	**1.0576**	**1.9920**	**0.2385**	2.583
	HHO	**0.9980**	1.5695	10.7632	1.6693	1.621
f_{15}	LHHO	**3.0756E-04**	**4.2473E-04**	**0.0012**	**2.4467E-04**	0.211
	HHO	3.1069E-04	4.2907E-04	0.0022	3.1794E-04	0.174
f_{16}	LHHO	**−1.0316**	**−1.0316**	**−1.0316**	**5.8700E-12**	0.214
	HHO	**−1.0316**	**−1.0316**	**−1.0316**	1.1081E-08	0.176
f_{17}	LHHO	**0.3979**	**0.3979**	**0.3979**	**1.7582E-09**	0.175
	HHO	**0.3979**	**0.3979**	0.3981	3.4854E-05	0.154
f_{18}	LHHO	**3.0000**	**3.0000**	**3.0000**	**3.2579E-09**	0.165
	HHO	**3.0000**	**3.0000**	3.0001	1.8747E-05	0.146
f_{19}	LHHO	**−3.8628**	**−3.8599**	**−3.8385**	**0.0055**	0.232
	HHO	**−3.8628**	−3.8566	−3.7803	0.0125	0.190
f_{20}	LHHO	**−3.2838**	**−3.0954**	**−2.8460**	**0.1039**	0.249
	HHO	−3.2752	−3.0650	−2.7811	0.1203	0.192
f_{21}	LHHO	**−10.1532**	**−8.1918**	**−5.0502**	**2.4818**	0.294
	HHO	−9.5677	−5.1354	−4.9901	0.6398	0.231
f_{22}	LHHO	**−10.4029**	**−9.1156**	**−5.0872**	**2.2866**	0.348
	HHO	−10.1150	−5.2464	−1.8243	1.2757	0.276
f_{23}	LHHO	**−10.5364**	**−8.7959**	**−5.1282**	**2.5415**	0.415
	HHO	−10.3041	−5.1765	−2.8004	0.8094	0.320

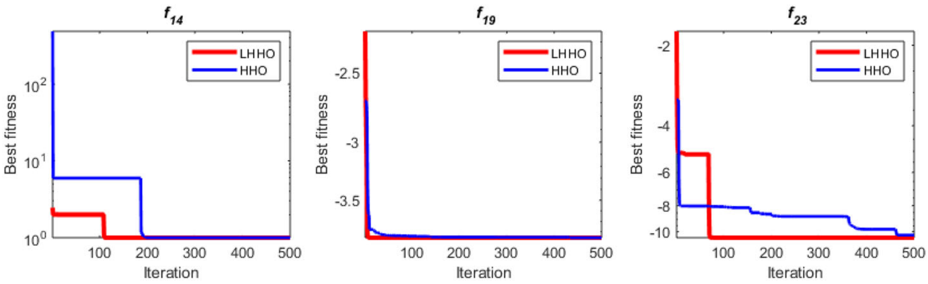

Fig. 4 Convergence curve of three multimodal test functions with fixed dimension

$$\begin{aligned}\varphi_0(s,t) &= \sum_{i=0}^{s_1-1}\sum_{j=0}^{t_1-1}p_{ij}\\ \varphi_1(s,t) &= \sum_{i=s_1}^{s_2-1}\sum_{j=t_2}^{t_2-1}p_{ij}\\ &\vdots\\ \varphi_K(s,t) &= \sum_{i=s_K}^{L-1}\sum_{j=t_K}^{L-1}p_{ij}\end{aligned} \tag{44}$$

where $i, j = 0, 1, \cdots, L-1$, and $\sum_{k=0}^{K}\varphi_k \approx 1$.

Then, the 2-D Masi entropy for the kth class ($H_k(s, t)$) is formulated as:

$$H_k(s,t) = \frac{1}{1-r}\log\left[1-(1-r)\sum_{i=s_k}^{s_{k+1}-1}\sum_{j=t_k}^{t_{k+1}-1}\left(\frac{p_{ij}}{\varphi_k(s,t)}\right)\log\left(\frac{p_{ij}}{\varphi_k(s,t)}\right)\right] \tag{45}$$

where $0 \le k \le K$, $s_0 = t_0 = 0$, $s_{K+1} = t_{K+1} = L-1$ and the entropic parameter r is set to 0.5.

The optimal threshold $\{s_1^* t_1^*, s_2^* t_2^*, \cdots, s_K^* t_K^*\}$ for 2-D Masi entropy-based multilevel image thresholding is formulated as a maximization criterion given as:

$$\{s_1^* t_1^*, s_2^* t_2^*, \cdots, s_K^* t_K^*\} = \text{argmax}[H_0(s,t) + H_1(s,t) + \cdots + H_K(s,t)] \tag{46}$$

subject to the conditions $0 < s_1 < s_2 < \cdots < s_K < L-1$, and $0 < t_1 < t_2 < \cdots < t_K < L-1$.

The maximization criterion presented in Eq. (46) is an exhaustive search of $O(L^{2K})$ computation, which increases exponentially when K increases. This can be resolved by a

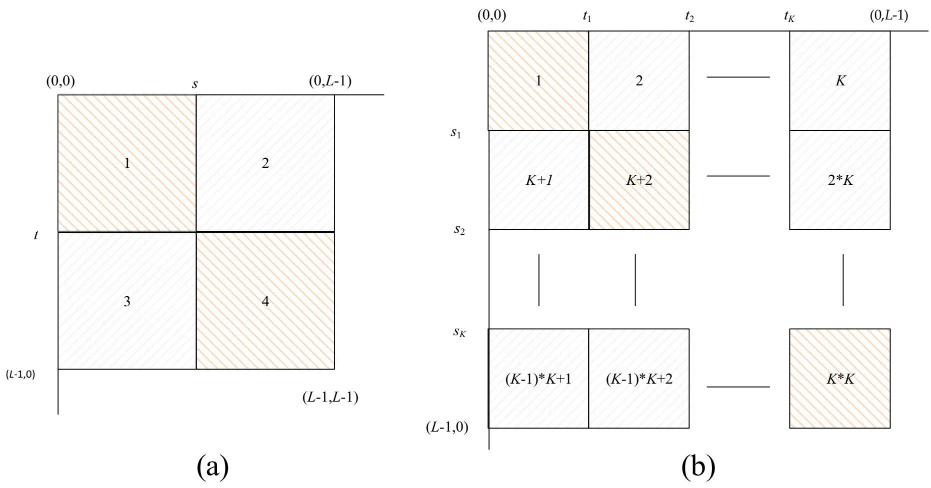

Fig. 5 2-D histogram plane **a** bi-level thresholding **b** multilevel image thresholding

Table 4 Experimental parameters for the various optimisation algorithms

Algorithm	Parameters
LHHO	N=20, t_{max}=100, β=1.5
HHO	N=20, t_{max}=100, β=1.5
CS	N=20, t_{max}=100, abandon probability p_a=0.25, step size α=1, and λ=1.5
PSO	N=20, t_{max}=100, inertia factor=0.3, c_1=2, and c_2=2
FA	N=20, t_{max}=100, α=0.5, β=0.2, and γ=1
WDO	N=20, t_{max}=100, RT coefficient=5, gravitational constant=0.2, constant in the update equation=0.5, Coriolis effect=0.4 and maximum allowed speed=0.3
STOA	N=20, t_{max}=100
DE	N=20, t_{max}=100, scaling factor F=0.5, and crossover probability C_r=0.9

good optimizer, which is fast and good enough to get the optimal solutions. Therefore, the newly proposed LHHO is used as a maximizer to obtain the optimal threshold values using Eq. (46) as an objective function.

5 Results and discussions

The proposed LHHO algorithm is used to obtain the optimal threshold values for the multilevel image thresholding. The suggested evolutionary-based multilevel image thresholding approach using 2-D Masi entropy is implemented. Some well-known evolutionary algorithms such as – HHO [19], CS [1], PSO [72], FA [22], WDO [8], STOA [10], and DE [57] are also used for a comparison to enrich the claim. It is noteworthy to mention here that the 1-D Masi entropy-based multilevel image thresholding technique is also implemented for a comparison. The validation of the

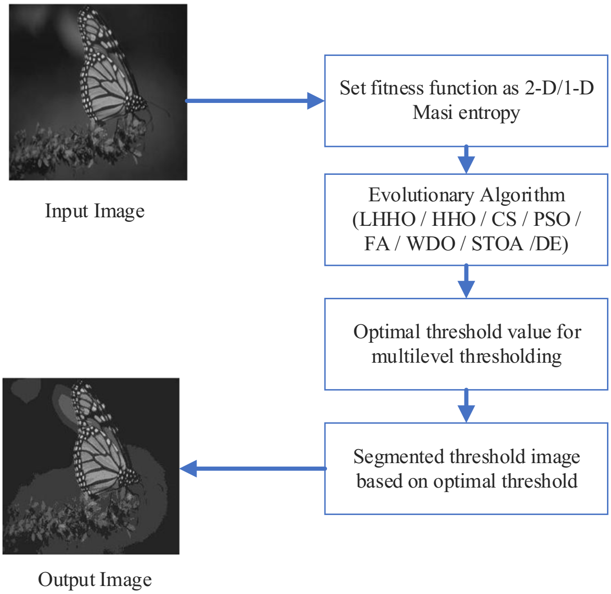

Fig. 6 Block diagram of the 2D/1D Masi entropy-based multilevel image thresholding using an evolutionary algorithm

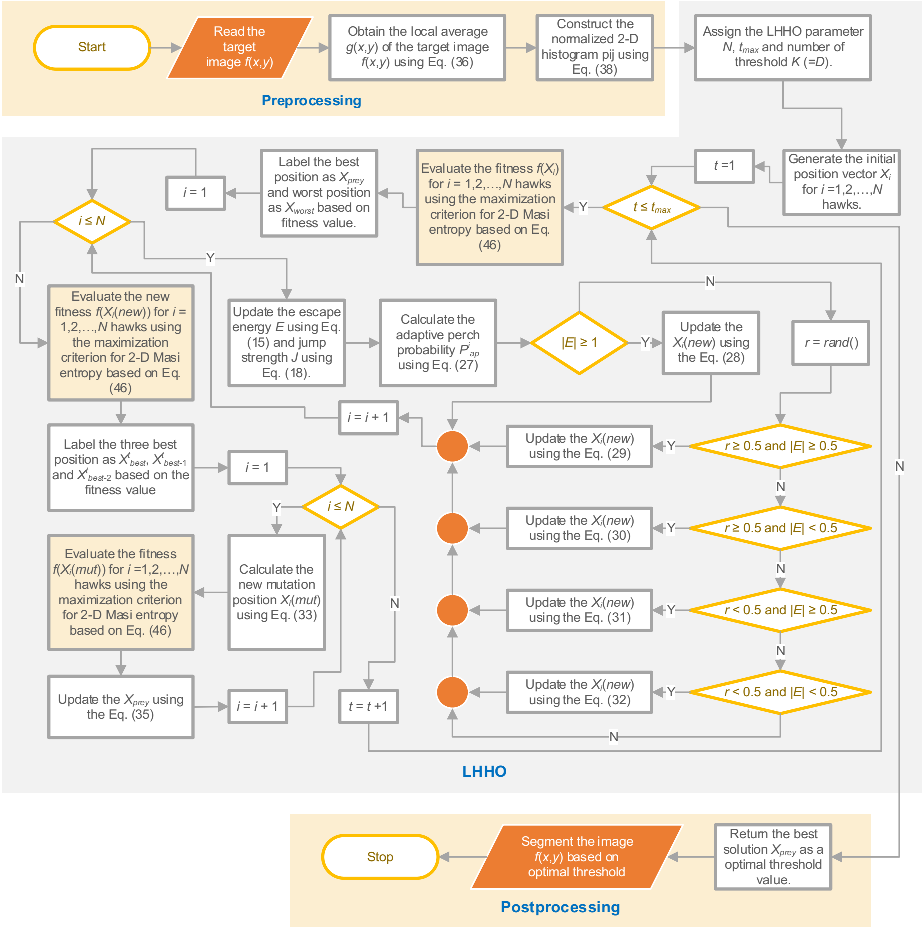

Fig. 7 Flowchart of the 2-D Masi entropy-based multilevel image thresholding using LHHO

performance is carried out with the help of the Berkeley segmentation dataset (BSDS 500) [34]. For the experiment, the parameters for the above evolutionary optimization methods are chosen the same as reported by the original work and are displayed in Table 4.

The BSDS 500 consists of 500 images, an extended version of the BSDS 300 public benchmark dataset used for the segmentation, and boundary detection. The BSDS 500 consists of a dataset of 200 training images and 300 testing images, which are composed of color images of a dimension of 481×321 or 321×481. We resize the BSDS 500 images to 256×256. These are used to evaluate the performance of the various optimization algorithms using 2-D Masi and 1-D Masi entropy-based multilevel image thresholding techniques. The well-known performance metrics - peak signal to noise ratio (PSNR) [1], feature similarity (FSIM) [77], and structural similarity (SSIM) [79] are used for the multilevel image thresholding performance evaluation. Each algorithm passes through 10 independent runs for stability analysis. The block diagram

Table 5 Comparison of the statistical result of various optimization algorithms (Computed over 500 images from BSDS 500) for 2-D Masi and 1-D Masi entropy-based multilevel image thresholding

K	Algorithm	2-D Masi					1-D Masi				
		f_{avg}	Std	$PSNR_{avg}$	$SSIM_{avg}$	$FSIM_{avg}$	f_{avg}	Std	$PSNR_{avg}$	$SSIM_{avg}$	$FSIM_{avg}$
5	LHHO	**15.8160**	**0.6724**	**27.7836**	**0.8180**	**0.8398**	**3.0134**	**0.0513**	**27.2703**	**0.8199**	**0.8385**
	HHO	15.7802	0.6876	27.5726	0.8158	0.8392	2.9995	0.0522	26.7002	0.7971	0.8295
	CS	15.0158	0.8231	27.3292	0.8154	0.8351	2.9763	0.0519	26.4124	0.7959	0.8140
	PSO	15.4866	0.7413	27.5403	0.8177	0.8420	2.9998	0.0524	27.0769	0.8049	0.8310
	FA	15.4812	0.6845	27.1792	0.8069	0.8329	2.9426	0.0571	26.1259	0.8041	0.8200
	WDO	14.3773	0.7825	25.7008	0.7919	0.8052	2.8170	0.0754	25.1560	0.7804	0.7998
	STOA	15.6703	0.7120	27.0279	0.8056	0.8302	2.9965	0.0523	26.8953	0.8031	0.8291
	DE	15.5953	0.7194	27.6076	0.8223	0.8415	2.9609	0.0532	27.2038	0.8110	0.8340
3	LHHO	**7.8885**	**0.3402**	**24.7804**	**0.7491**	**0.7702**	**2.1419**	**0.0398**	**23.9673**	**0.7294**	0.7545
	HHO	7.8857	0.3408	23.6588	0.7189	0.7460	2.1410	0.0408	23.2393	0.7051	0.7441
	CS	7.7568	0.3722	24.0134	0.7343	0.7514	2.1375	0.0410	23.8206	0.7240	0.7476
	PSO	7.8486	0.3481	23.7952	0.7209	0.7544	2.1411	0.0408	23.5903	0.7156	0.7435
	FA	7.8489	0.3360	24.5364	0.7478	0.7680	2.1263	0.0460	23.7209	0.7256	**0.7574**
	WDO	7.6632	0.3503	24.0867	0.7314	0.7541	2.1095	0.0462	23.6307	0.7229	0.7496
	STOA	7.8675	0.3466	23.7437	0.7197	0.7527	2.1392	0.0408	23.7386	0.7212	0.7480
	DE	7.8583	0.3463	24.4514	0.7413	0.7635	2.1311	0.0434	23.6041	0.7168	0.7531
2	LHHO	**4.8701**	**0.2116**	**22.1705**	**0.6809**	**0.7089**	**1.6782**	**0.0352**	**21.8540**	**0.6678**	0.6993
	HHO	4.8618	0.2159	22.1113	0.6724	0.7028	1.6764	0.0356	21.6442	0.6648	**0.6994**
	CS	4.8371	0.2228	21.3309	0.6501	0.6796	1.6760	0.0357	21.2969	0.6487	0.6796
	PSO	4.8569	0.2175	21.3455	0.6486	0.6785	1.6739	0.0361	21.2325	0.6463	0.6878
	FA	4.8548	0.2182	22.1416	0.6753	0.7008	1.6722	0.0380	21.2674	0.6478	0.6788
	WDO	4.8258	0.2205	21.7496	0.6572	0.6868	1.6728	0.0364	21.0807	0.6343	0.6800
	STOA	4.8585	0.2171	21.5834	0.6559	0.6857	1.6756	0.0357	21.5194	0.6552	0.6936
	DE	4.8359	0.2189	21.9417	0.6741	0.6899	1.6787	0.0377	21.0689	4.8323	0.2189

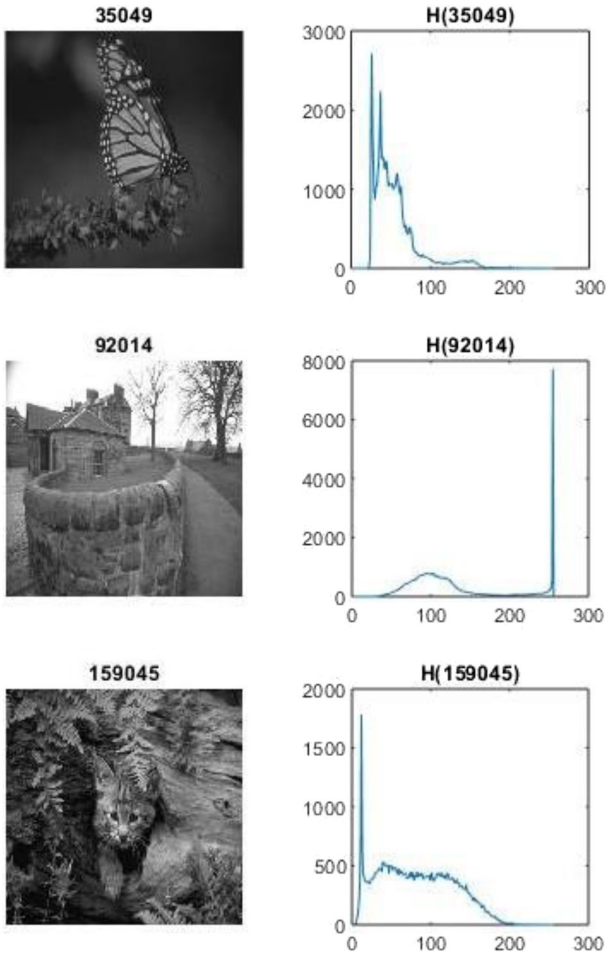

Fig. 8 Sample test images (with identification number 35049, 92014, and 159,045) and their corresponding histograms

of the evolutionary algorithm for the multilevel image thresholding is shown in Fig. 6. Flowchart of the 2-D Masi entropy-based multilevel image thresholding using the LHHO is displayed in Fig. 7.

A deeper insight into the statistical analysis is provided here. The 2-D Masi and 1-D Masi entropy-based multilevel image thresholding methods are optimization (maximization) problems as described by Eqs. (13) and (46). Usually, PSNR, FSIM and SSIM metrics are used for result analysis. For a more detail analysis of the results, we supplement the statistical results with average fitness value 'f_{avg}' and a standard deviation '*Std*'. Note that the average fitness value and the standard deviation are computed among 10 independent runs. Here, we use threshold levels K as 2, 3, and 5 for an analysis. As the multilevel image thresholding problem is a maximization problem, the highest average fitness value (f_{avg}) is calculated using the best fitness values among 10 independent runs. The other parameters – average PSNR ($PSNR_{avg}$), average FSIM ($FSIM_{avg}$) and average SSIM ($SSIM_{avg}$) are calculated from the best threshold

Table 6 Statistical results of various optimization algorithms for a subject with the identification number 35049 from BSDS 500 on 2-D Masi and 1-D Masi entropy-based multilevel image thresholding

K	Method	Parameter	Algorithm							
			LHHO	HHO	CS	PSO	FA	WDO	STOA	DE
5	2-D Masi	f_{avg}	**14.6966**	14.6932	13.2617	14.4846	14.2200	14.4235	12.7739	14.1931
		Std	**0.0261**	0.0347	0.4596	0.0905	0.4514	0.0675	0.7416	0.1388
		f_{best}	**14.7340**	14.7226	13.8419	14.5993	14.6953	14.6098	13.9621	14.4116
		Opt. Th.	**47, 68, 84, 124, 141**	50, 77, 119, 149, 172	41, 83, 122, 143, 192	54, 82, 118, 144, 166	47. 66, 83, 102, 125	48, 77, 97, 131, 164	52, 65, 80, 94, 107	56, 69, 95, 126, 143
		$PSNR_{best}$	**31.0657**	30.1644	29.2185	29.6716	31.0637	30.5743	29.4685	29.1324
		$SSIM_{best}$	0.9182	0.9037	0.8889	0.9006	**0.9219**	0.9093	0.9135	0.9004
		$FSIM_{best}$	0.8866	0.8759	0.8568	0.8724	**0.8868**	0.8802	0.8729	0.8523
	1-D Masi	f_{avg}	**3.0028**	2.9940	2.9578	2.9929	2.8549	2.9146	2.6278	3.0023
		Std	**0.0096**	0.0164	0.0167	0.0135	0.606	0.0280	0.1081	0.0167
		f_{best}	**3.0189**	3.0165	2.9903	3.0095	2.9416	2.9608	2.7708	3.0189
		Opt. Th.	**49, 78, 124, 156, 190**	48, 79, 119, 166, 207	56, 99, 140, 183, 213	61, 96, 131, 169, 209	53, 77, 96, 114, 136	63, 97, 121, 150, 175	63, 95, 129, 165, 209	62, 94, 124, 164, 210
		$PSNR_{best}$	**29.9725**	29.9588	28.2404	27.7714	29.8607	27.5160	27.4554	27.6716
		$SSIM_{best}$	0.9008	0.9016	0.8774	0.8770	**0.9087**	0.8774	0.8758	0.8773
		$FSIM_{best}$	0.8698	0.8686	0.8454	0.8534	**0.8803**	0.8599	0.8567	0.8554
3	2-D Masi	f_{avg}	**7.3619**	7.3602	7.0957	7.3211	7.3280	7.3214	6.9482	7.3031
		Std	**0.0026**	0.0048	0.1105	0.0251	0.0211	0.0127	0.2827	0.0206
		f_{best}	**7.3637**	7.3636	7.2563	7.3554	7.3612	7.3429	7.2862	7.3463
		Opt. Th.	**51, 80, 121**	76, 116, 153	76, 115, 153	73, 125, 160	74, 107, 139	66, 104, 148	73,100, 125	72, 109, 136
		$PSNR_{best}$	**29.1280**	25.4260	25.4260	25.6499	25.7224	26.6223	25.8262	25.9658
		$SSIM_{best}$	**0.8978**	0.8515	0.8515	0.8489	0.8560	0.8702	0.8582	0.8595
		$FSIM_{best}$	**0.8631**	0.8105	0.8106	0.8112	0.8176	0.8443	0.8185	0.8234
	1-D Masi	f_{avg}	**2.1374**	2.1369	2.1288	2.1227	2.0940	2.1097	2.0403	2.1346
		Std	**5.2188E-04**	0.0009	0.0039	0.0097	0.0362	0.0124	0.0514	0.0012
		f_{best}	**2.1374**	2.1373	2.1363	2.1369	2.1216	2.1334	2.1072	2.1371
		Opt. Th.	**42, 86, 160**	76, 119, 167	78, 158, 200	82, 163, 209	75, 116, 169	71, 123, 171	82, 137, 171	82, 164, 209
		$PSNR_{best}$	**27.2205**	25.3901	24.0986	23.9681	25.5187	25.8684	24.7564	23.9525
		$SSIM_{best}$	**0.8685**	0.8501	0.8280	0.8264	0.8512	0.8540	0.8389	0.8264
		$FSIM_{best}$	**0.8324**	0.8075	0.7912	0.7858	0.8097	0.8172	0.7951	0.7858

Table 6 (continued)

K	Method	Parameter	Algorithm							
			LHHO	HHO	CS	PSO	FA	WDO	STOA	DE
2	2-D Masi	f_{avg}	**4.5099**	**4.5099**	4.4676	4.5033	4.5025	4.5055	4.4093	4.5015
		Std	**4.4073E-05**	7.2102E-05	0.0209	0.0041	0.0112	0.0021	0.0853	0.0041
		f_{best}	**4.5099**	**4.5099**	4.5017	4.5088	4.5088	4.5089	4.4921	4.5078
		Opt. Th.	**51, 91**	**51, 91**	88, 147	78, 127	75, 113	90, 139	82, 138	90, 136
		$PSNR_{best}$	**26.9611**	**26.9611**	24.1793	24.9734	25.2543	24.1911	24.5997	24.2233
		$SSIM_{best}$	**0.8718**	**0.8718**	0.8237	0.8454	0.8492	0.8236	0.8368	0.8246
		$FSIM_{best}$	**0.8337**	**0.8337**	0.7818	0.8004	0.8071	0.7805	0.7930	0.7811
	1-D Masi	f_{avg}	**1.6664**	**1.6664**	1.6654	**1.6644**	1.6281	1.6592	1.6403	**1.6664**
		Std	**0**	**0**	6.3275E-04	**0**	0.0304	0.0147	0.0202	**0**
		f_{best}	**1.6664**	**1.6664**	1.6662	**1.6664**	1.6653	1.6662	1.6637	**1.6664**
		Opt. Th.	**75, 125**	80, 164	79, 165	82, 167	83, 164	79, 165	89, 182	82, 167
		$PSNR_{best}$	**25.2293**	23.9117	23.9302	23.9117	23.9329	23.9302	23.7267	23.9117
		$SSIM_{best}$	**0.8459**	0.8269	0.8269	0.8262	0.8244	0.8269	0.8163	0.8262
		$FSIM_{best}$	**0.8053**	0.7878	0.7885	0.7851	0.7844	0.7885	0.7739	0.7851

Table 7 Statistical results of various optimization algorithms for a subject with identification number 92014 from BSDS 500 on 2-D Masi and 1-D Masi entropy-based multilevel image thresholding

K	Method	Parameter	Algorithm							
			LHHO	HHO	CS	PSO	FA	WDO	STOA	DE
5	2-D Masi	f_{avg}	**15.9488**	15.9450	15.0260	15.9154	15.2311	15.7034	13.6875	15.5933
		Std	**0.0379**	0.0687	0.3743	0.0393	0.1755	0.1326	0.5471	0.1008
		f_{best}	**15.9873**	15.9888	15.6924	15.9558	15.5156	15.8819	14.7351	15.7871
		Opt. Th.	**84, 110, 141, 192, 233**	81, 117, 149, 193, 234	64, 106, 137, 185, 206	83, 112, 158, 214, 237	61, 98, 134, 170, 212	72, 107, 138, 185, 233	107, 121, 146, 173, 194	65, 100, 133, 170, 218
		$PSNR_{best}$	**29.0065**	28.5595	27.4423	28.2867	28.0465	28.8834	25.4016	28.5197
		$SSIM_{best}$	**0.8352**	0.8210	0.8018	0.8224	0.8147	0.8320	0.7497	0.8240
		$FSIM_{best}$	0.8620	0.8587	0.8361	0.8548	0.8508	**0.8697**	0.7786	0.8612
	1-D Masi	f_{avg}	**2.8742**	2.8708	2.8361	2.8708	2.7437	2.7827	2.5326	2.8709
		Std	**0.0022**	0.0043	0.0131	0.0036	0.0446	0.0334	0.0947	0.0041
		f_{best}	**2.8759**	2.8758	2.8593	2.8742	2.8165	2.8370	2.6841	2.8762
		Opt. Th.	**81, 113, 142, 183, 222**	27, 73, 111, 151, 203	24, 78, 116, 147, 217	26, 87, 128, 168, 212	82, 111, 136, 159, 183	30, 76, 109, 149, 204	107, 122, 151, 165, 176	26, 71, 110, 150, 204
		$PSNR_{best}$	**28.8461**	27.1850	27.2279	26.9091	26.9541	27.4654	24.4798	27.1301
		$SSIM_{best}$	**0.8293**	0.7992	0.8046	0.7809	0.8176	0.8104	0.7328	0.7973
		$FSIM_{best}$	**0.8585**	0.8327	0.8376	0.8108	0.8388	0.8395	0.7609	0.8310
3	2-D Masi	f_{avg}	**7.8625**	7.8490	7.7214	7.8570	7.7302	7.8395	7.5363	7.8214
		Std	**0.0120**	0.0250	0.0432	0.0028	0.0908	0.0173	0.2007	0.0183
		f_{best}	**7.8669**	7.8666	7.7950	7.8602	7.8291	7.8625	7.7706	7.8545
		Opt. Th.	**92,143, 207**	98, 150, 213	88, 133, 176	97, 150, 213	95, 137, 178	93, 143, 204	100, 128, 221	100, 155, 216
		$PSNR_{best}$	**25.6140**	25.5139	24.8959	25.5233	24.9591	25.6067	24.6199	25.3970
		$SSIM_{best}$	**0.7454**	0.7381	0.7464	0.7375	0.7405	0.7426	0.7319	0.7321
		$FSIM_{best}$	**0.7703**	0.7666	0.7680	0.7654	0.7615	0.7669	0.7667	0.7628
	1-D Masi	f_{avg}	**2.0220**	2.0202	2.0077	2.0182	1.9639	1.9755	1.9418	2.0214
		Std	**4.5563E-16**	0.0027	0.0073	0.0110	0.0159	0.0197	0.0276	0.0010
		f_{best}	**2.0220**	2.0220	2.0181	2.0220	2.0213	2.0217	1.9785	2.0220
		Opt. Th.	**96, 147, 204**	105, 161, 227	25, 74, 139	82, 137, 194	94, 145, 196	90,144, 200	27, 82, 132	27,79, 124
		$PSNR_{best}$	**25.5245**	25. 0748	20.2122	25.1020	25.4279	25.4378	19.5154	18.0118
		$SSIM_{best}$	0.7373	0.7241	0.6473	**0.7401**	0.7381	0.7398	0.6576	0.6321
		$FSIM_{best}$	0.7627	0.7598	0.6736	**0.7658**	0.7605	0.7638	0.6828	0.6695

Table 7 (continued)

K	Method	Parameter	Algorithm							
			LHHO	HHO	CS	PSO	FA	WDO	STOA	DE
2	2-D Masi	f_{avg}	**4.7895**	4.7894	4.7559	4.7876	4.7690	7.7864	4.7401	4.7844
		Std	**3.0711E-04**	5.8458E-04	0.0152	0.0015	0.0291	0.0015	0.0434	0.0025
		f_{best}	**4.7898**	4.7898	4.7828	4.7892	4.7881	4.7888	4.7886	4.7883
		Opt. Th.	**103, 183**	101, 178	135, 202	131, 197	125, 180	131, 200	130, 201	130, 199
		$PSNR_{best}$	**23.5327**	23.5038	22.0627	22.2271	22.4101	22.2341	22.2815	22.2783
		$SSIM_{best}$	0.6846	**0.6867**	06132	0.6222	0.6309	0.6228	0.6245	0.6248
		$FSIM_{best}$	**0.7100**	**0.7100**	0.6542	0.6598	0.6664	0.6614	0.6635	0.6631
	1-D Masi	f_{avg}	**1.5813**	1.5812	1.5781	1.5812	1.5523	1.5511	1.5453	1.5812
		Std	**3.7250E-05**	2.3775E-04	0.0032	4.9256E-04	0.0068	0.0162	0.0154	0.0004
		f_{best}	**1.5813**	**1.5813**	1.5812	**1.5813**	**1.5813**	1.5769	1.5812	**1.5813**
		Opt. Th.	**91, 138**	134, 188	27, 121	27, 110	79, 124	134, 184	27, 116	27, 109
		$PSNR_{best}$	**20.5003**	22.0020	16.9121	15.5548	18.0116	21.9359	16.2295	15.4515
		$SSIM_{best}$	**0.6729.**	0.6125	0.5271	0.5271	0.6320	0.6103	0.5265	0.5264
		$FSIM_{best}$	**0.6958**	0.6497	0.5698	0.5837	0.6694	0.6477	0.5758	0.5845

Table 8 Statistical results of various optimization algorithms for a subject with identification number 159045 from BSDS 500 on 2-D Masi and 1-D Masi entropy-based multilevel image thresholding

K	Method	Parameter	Algorithm							
			LHHO	HHO	CS	PSO	FA	WDO	STOA	DE
5	2-D Masi	f_{avg}	**16.2865**	16.1742	15.2199	16.1647	15.8377	16.0426	14.4374	15.8906
		Std	**0.0090**	0.0345	0.3593	0.0541	0.2335	0.0634	0.5932	0.1215
		f_{best}	**16.2948**	16.2933	15.7234	16.2582	16.1530	16.1246	15.8563	16.0588
		Opt. Th.	**36, 64, 91, 120, 151**	47, 87, 126, 168, 208	35, 70, 115, 137, 224	55, 89, 122, 150, 190	44, 70, 92, 112, 131	47, 83, 113, 135, 159	53, 84, 96, 124, 134	44, 70, 103, 129, 162
		$PSNR_{best}$	**29.3311**	26.8476	27.2480	27.0350	28.1832	28.1630	27.0784	28.6693
		$SSIM_{best}$	**0.8868**	0.8178	0.8431	0.8201	0.8639	0.8554	0.8285	0.8673
		$FSIM_{best}$	**0.9101**	0.8558	0.8614	0.8605	0.8684	0.8855	0.8427	0.8947
	1-D Masi	f_{avg}	**3.0226**	3.0224	2.9955	3.0218	2.9079	2.9775	2.6938	3.0239
		Std	**0.0016**	0.0022	0.0097	0.0019	0.0493	0.0282	0.1163	0.0018
		f_{best}	**3.0259**	3.0259	3.0158	3.0239	2.9929	3.0154	3.0105	3.0260
		Opt. Th.	**37, 72, 101, 129, 164**	58, 98, 133, 162, 184	42, 88, 121, 159, 206	47, 85, 122, 168, 208	44, 80, 122, 159, 211	40, 75, 105, 149, 184	64, 88, 97, 115, 134	47, 85, 123, 167, 209
		$PSNR_{best}$	**28.8662**	26.3823	27.0381	26.8800	27.2112	27.7998	25.9869	26.9167
		$SSIM_{best}$	**0.8743**	0.7991	0.8258	0.8185	0.8299	0.8454	0.7943	0.8197
		$FSIM_{best}$	**0.9041**	0.8486	0.8635	0.8534	0.8654	0.8835	0.8187	0.8550
3	2-D Masi	f_{avg}	**8.1540**	8.1539	7.9793	8.1342	8.0853	8.1312	7.8139	8.1081
		Std	**6.6846E-04**	9.0766E-04	0.0698	0.0122	0.0651	0.0087	0.2747	0.0125
		f_{best}	**8.1548**	8.1546	8.1043	8.1509	8.1519	8.1479	8.0698	8.1277
		Opt. Th.	**30, 76, 115**	63, 97, 121	68, 122, 174	66, 112, 152	54, 88, 115	73, 124, 165	85, 128, 164	71, 110, 155
		$PSNR_{best}$	**25.3738**	24.9552	23.9342	24.8002	25.2611	23.8588	23.3709	24.4339
		$SSIM_{best}$	**0.7906**	0.7554	0.7060	0.7431	0.7719	0.7044	0.6848	0.7259
		$FSIM_{best}$	**0.8065**	0.7816	0.7574	0.7949	0.7893	0.7654	0.7529	0.7828
	1-D Masi	f_{avg}	**2.1588**	2.1587	2.1541	2.1590	2.1060	2.1504	2.0626	2.1591
		Std	**6.3642E-04**	6.6083E-04	0.0026	1.0442E-04	0.0182	0.0056	0.0582	2.8256E-05
		f_{best}	**2.1591**	2.1591	2.1587	2.1591	2.1531	2.1586	2.1576	2.1591
		Opt. Th.	**59, 120, 211**	70, 133, 208	60, 116, 205	72, 131, 207	69, 128, 202	70, 133, 207	44, 121, 204	70, 131, 207
		$PSNR_{best}$	**23.5777**	23.1555	23.7121	23.2209	23.4008	23.1604	22.5873	23.2519
		$SSIM_{best}$	**0.6975**	0.6713	0.7020	0.6732	0.6831	0.6719	0.6733	0.6754
		$FSIM_{best}$	**0.7300**	0.7195	0.7346	0.7220	0.7269	0.7202	0.7108	0.7221

values obtained from the best fitness value among 10 independent runs. Finally, these results

Table 8 (continued)

K	Method	Parameter	Algorithm							
			LHHO	HHO	CS	PSO	FA	WDO	STOA	DE
2	2-D Masi	f_{avg}	**5.0378**	5.0378	5.0093	5.0352	5.0269	5.0357	4.9930	5.0319
		Std	**1.2419E-05**	3.5554E-05	0.0146	0.0024	0.0228	9.7099E-04	0.0413	0.0027
		f_{best}	**5.0378**	5.0378	5.0255	5.0374	5.0378	5.0374	5.0322	5.0351
		Opt. Th.	**65, 122**	92, 152	84, 153	70, 137	63, 128	72, 125	79, 148	91, 145
		$PSNR_{best}$	**23.5725**	21.5206	21.9077	22.9376	23.3224	23.3634	22.8149	21.7723
		$SSIM_{best}$	**0.6941**	0.5921	0.6066	0.6631	0.6863	0.6819	0.6540	0.6080
		$FSIM_{best}$	**0.7296**	0.6736	0.6808	0.7132	0.7249	0.7254	0.7114	0.6849
	1-D Masi	f_{avg}	**1.6842**	1.6840	1.6834	1.6842	1.6558	1.6614	1.6652	1.6842
		Std	**4.5563E-16**	2.9337E-04	8.2601E-04	2.0588E-06	0.0108	0.0142	0.0132	2.0588E-06
		f_{best}	**1.6842**	1.6842	1.6842	1.6842	1.6842	1.6839	1.6836	1.6842
		Opt. Th.	**46, 101**	94,207	86, 207	94, 207	81, 131	93, 148	94, 207	94, 207
		$PSNR_{best}$	**23.3672**	20.3936	20.5638	20.3936	22.7903	21.5523	20.3936	20.3936
		$SSIM_{best}$	**0.7034**	0.5201	0.5271	0.5201	0.6550	0.5973	0.5201	0.5201
		$FSIM_{best}$	**0.7275**	0.5836	0.5882	0.5836	0.7110	0.6786	0.5836	0.5836

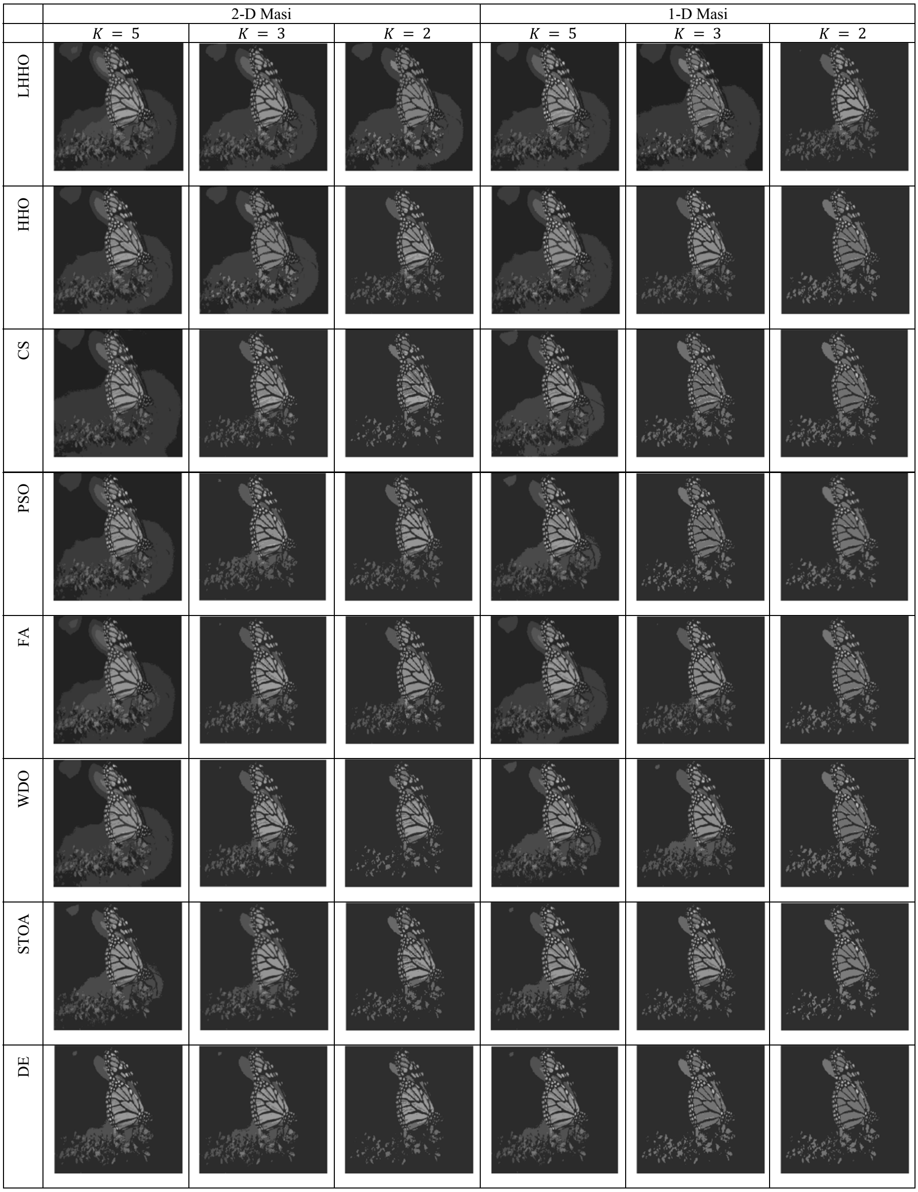

Fig. 9 Thresholded images of the subject with identification number 35049 from BSDS 500 on 2-D Masi and 1-D Masi entropy-based multilevel image thresholding using various optimization algorithms for $K = 2, 3, 5$

are computed over 500 images considering the best fitness values among 10 independent runs. The results are good, as opposed to the earlier algorithms, encourage future applications.

The performance of the LHHO and other optimization algorithms in all 500 images considered from BSDS 500 is presented in Table 5. Statistical results computed over 500 images from BSDS 500 dataset are presented for analysis and interpretation. From a

Fig. 10 Thresholded images of a subject with identification number 92014 from BSDS 500 on 2-D Masi and 1-D Masi entropy-based multilevel image thresholding in various optimization algorithms for $K = 2, 3, 5$

comparison of the statistical parameters, the evolutionary 2-D Masi entropy-based multilevel image thresholding achieves better results than the 1-D Masi entropy-based multilevel image thresholding. For instance, an increase of about 2% to 4% is observed in the case of $PSNR_{avg}$ values for K = 5. A similar trend is followed for other threshold levels. The reason behind such an improvement could be the inclusion of the contextual information. From Table 5, it is envisioned that the LHHO based multilevel image

Fig. 11 Thresholded images of a subject with identification number 159045 from BSDS 500 on 2-D Masi and 1-D Masi entropy-based multilevel image thresholding in various optimization algorithms for $K = 2, 3, 5$

thresholding approach performs well compared with state-of-the-art optimization methods. Even more interesting is its consistent 'Std' data. Need to mention here that the computation over 500 images highlights its capability to solve image segmentation problems.

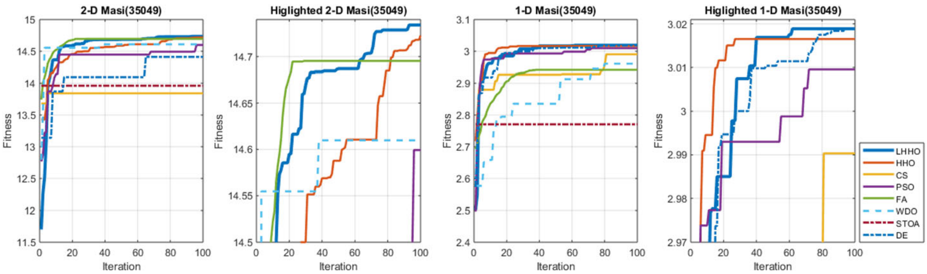

Fig. 12 Convergence curves of various optimization algorithms with identification number 35049 from BSDS 500 using 2-D Masi and 1-D Masi entropy-based multilevel image thresholding for $K = 5$

Exemplary results are provided here to ensure its usefulness for such applications. To provide a more in-depth analysis of the proposed method, three subjects from BSDS 500 with identification number 35049, 92014, and 159,045 are used for the experiment. To encourage readers, these examples are good enough to analyze and interpret. The sample subjects with the corresponding histograms are presented in Fig. 8. For the statistical parameter analysis together with 'f_{avg}' and 'Std', we use the best fitness value f_{best} among 10 independent runs. The 'Opt. Th.' parameter is the optimal threshold value obtained using an optimizer. The '$PSNR_{best}$', '$SSIM_{best}$' and '$FSIM_{best}$' are the PSNR, SSIM, and FSIM values obtained by using the optimal threshold values. The good results primarily depend on the optimal threshold values. Especially, the role of an optimizer is crucial. Other factors influencing the good results are the contextual information and the inherent characteristics of images. In this context, nevertheless, it is justified to achieve the results presented here.

The statistical result of the subject 35,049 is presented in Table 6 while the results of the subject 92,014 and the subject 159,045 are displayed in Tables 7 and 8, respectively. From Tables 6, 7 and 8, it is seen that the evolutionary 2-D Masi entropy-based method using the LHHO outperforms than other techniques. The corresponding threshold images for subject 35,049, 92,014, and 159,045 are shown in Figs. 9, 10, and 11, respectively. It is observed that the best threshold image is the top left corner image that is corresponding to the evolutionary 2-D Masi entropy-based multilevel image thresholding using the LHHO. The different regions are clearly visible, because of the more visual information. The convergence curves (fitness vs. iteration) for the threshold level K = 5 are shown in Figs. 12, 13, and 14 for the subjects 35,049, 92,014, and 159,045, respectively. The proposed inbuilt mechanisms enforce the LHHO for a rapid convergence. Furthermore, the suggested algorithm takes a smaller number of iterations than other state-of-the-art methods. From this analysis, it is seen that the evolutionary 2-D Masi entropy-based multilevel image thresholding using the LHHO has inherent potential for the future applications in image processing.

The suggested LHHO has shown better results than state-of-the-art optimizers, because it inherits adaptive perching and mutation-selection mechanism to enhance the exploration. It is reiterated that the exploitation remains unchanged. Due to quick dispersal of the position of the Harris hacks in the search space, it converges towards optimal solution rapidly even with a lesser number of the iteration count. Nonetheless, the results obtained using 2-D Masi entropy-

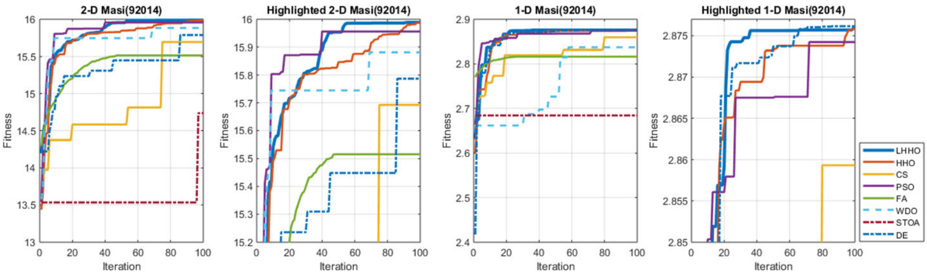

Fig. 13 Convergence curves of various optimization algorithms with identification number 92014 from BSDS 500 using 2-D Masi and 1-D Masi entropy-based multilevel image thresholding for $K = 5$

based method is better than the 1-D Masi technique, because the contextual information is enshrined.

6 Conclusions

In this work, a leader Harris hawks optimization (LHHO) algorithm is proposed to enhance the exploration capability of the HHO without reducing the exploitation capacity by inhibiting the adaptive perch probability and a leader-based mutation-selection approach. The LHHO showed better performance than the HHO when compared with well-known benchmark functions for function optimizations; both on quantitative (i.e. Best, Avg, Worst, and Std) and qualitative (i.e., convergence curve) performances. The LHHO is computationally expensive as compared to HHO, due to additional learning taking place via leader-based mutation-selection for a better optimal solution, is the only drawback. However, the convergence is faster, because it takes less number of iterations than the HHO. The LHHO can be used to solve the optimization problems in the different fields of engineering. In this work, the LHHO is tested on a single-objective problem, which may be further extended to a multi-objective problem. The possible future extension of the LHHO would be in opposition-based learning, chaos-based phases, and general type-2 fuzzy-based learning.

Further, the LHHO is used in the multilevel image thresholding to demonstrate its ability in image segmentation. For the image segmentation problem, in this work, a 2-D Masi entropy objective function (for multilevel image thresholding) is proposed. The 2-D Masi entropy is based on the underlying principle of 1-D Masi entropy and the advantage of the 2-D histogram, utilizes the contextual information during the thresholding process. Further, a proposal of an evolutionary 2-D Masi entropy-based multilevel image thresholding using the LHHO is suggested. Our proposal yields superior results than the 1-D Masi entropy-based method, because it extracts the contextual information efficiently. The comparison of various methods is made by using well-known performance metrics – PSNR, FSIM, and SSIM (in this article). The state-of-the-art algorithms are also used to envisage the effectiveness of the LHHO based multilevel image thresholding, which reveals that the LHHO quickly obtains the optimal threshold values in terms of the iteration count. There are merits in the proposal. To figure out, it provides us efficient segmentation results, a faster

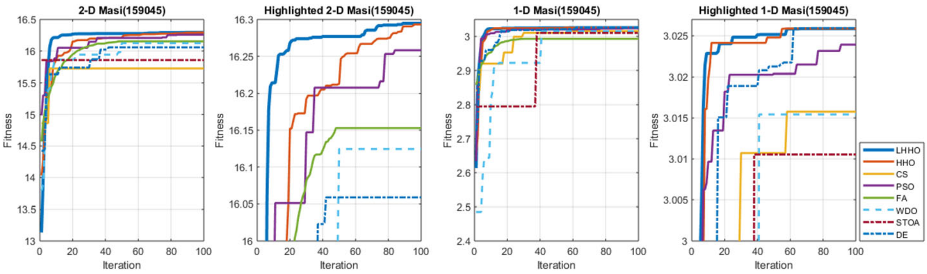

Fig. 14 Convergence curves of various optimization algorithms with identification number 159045 from BSDS 500 using 2-D Masi and 1-D Masi entropy-based multilevel image thresholding for $K = 5$

convergence, and attractive for ready implementations. The future scope of the work would be the multispectral image analysis, image compression, object detection, biomedical image segmentation, and in more general where we require computational intelligence-based image segmentation.

Appendix 1. Test functions

Table 9 Unimodal benchmark functions

Function	D	Range	f_{min}
$f_1(X) = \sum_{i=1}^{D} x_i^2$	30, 100	$[-100, 100]^D$	0
$f_2(X) = \sum_{i=1}^{D} \lvert x_i \rvert + \prod_{i=1}^{D} \lvert x_i \rvert$	30, 100	$[-10, 10]^D$	0
$f_3(X) = \sum_{i=1}^{D} \left(\sum_{j=1}^{i} x_j \right)^2$	30, 100	$[-100, 100]^D$	0
$f_4(X) = \max_i \{ \lvert x_i \rvert, 1 \le i \le D \}$	30, 100	$[-100, 100]^D$	0
$f_5(X) = \sum_{i=1}^{D-1} \left[100 \left(x_{i+1} - x_i^2 \right)^2 + (x_i - 1)^2 \right]$	30, 100	$[-30, 30]^D$	0
$f_6(X) = \sum_{i=1}^{D} (\lfloor x_i + 0.5 \rfloor)^2$	30, 100	$[-100, 100]^D$	0
$f_7(X) = \sum_{i=1}^{D} i x_i^4 + random[0, 1)$	30, 100	$[-1.28, 1.28]^D$	0

Table 10 Multimodal benchmark functions with varied dimension

Function	D	Range	f_{min}
$f_8(X)=\sum_{i=1}^{D}-x_i\sin\left(\sqrt{\lvert x_i\rvert}\right)$	30, 100	$[-500,500]^D$	$-418.9829\times D$
$f_9(X)=\sum_{i=1}^{D}\left[x_i^2-10\cos(2\pi x_i)\ +10\right]$	30, 100	$[-5.12,5.12]^D$	0
$f_{10}(X)=-20\exp\left(-0.2\sqrt{\frac{1}{d}\sum_{i=1}^{D}x_i^2}\right)-\exp\left(\frac{1}{d}\sum_{i=1}^{D}\cos(2\pi x_i)\right)+20+e$	30, 100	$[-32,32]^D$	0
$f_{11}(X)=\frac{1}{4000}\sum_{i=1}^{D}x_i^2-\prod_{i=1}^{D}\cos\left(\frac{x_i}{\sqrt{i}}\right)+1$	30, 100	$[-600,600]^D$	0
$f_{12}(X)=\frac{\pi}{D}\left\{10\sin(\pi y_i)+\sum_{i=1}^{D-1}(y_i-1)^2\left[1+10\sin^2\left(\pi y_{i+1}\right)\right]+(y_D-1)^2\right\}+\sum_{i=1}^{D}u(x_i,10,100,4)$	30, 100	$[-50,50]^D$	0
$y_i=1+\frac{x_i+1}{4}u(x_i,a,k,m)=\{\,k(x_i-a)\ ^m x_i>a\ 0-a<x_i<a\ k(-x_i-a)\ ^m x_i<-a$			
$f_{13}(X)=0.1\left\{\sin^2(3\pi x_1)\ +\sum_{i=1}^{D}(x_i-1)\ ^2\left[1+\sin^2(3\pi x_i+1)\right]\ +(x_D-1)\ ^2\left[1+\sin^2(2\pi x_D)\right]\right\}\ +\sum_{i=1}^{D}u(x_i,5,100,4)$	30, 100	$[-50,50]^D$	0
$y_i=1+\frac{x_i+1}{4}u(x_i,a,k,m)=\{\,k(x_i-a)\ ^m x_i>a\ 0-a<x_i<a\ k(-x_i-a)\ ^m x_i<-a$			

Table 11 Multimodal benchmark functions with fixed dimension

Function	Range	f_{min}
$f_{14}(X) = \left(\frac{1}{500} + \sum_{j=1}^{25} \frac{1}{j+\sum_{i=1}^{2}\left(x_i - a_{ij}\right)}\ ^6\right)^{-1}$ $a_{ij} = (-32\quad -16\quad 0\quad 16\quad 32\quad -32\quad \cdots\quad 0\quad 16\quad 32\ -32 -32 -32 -32 -32$ $-16 \cdots 323232)$	$[-65.536,\ 65.536]^2$	1
$f_{15}(X) = \sum_{i=1}^{11}\left[a_i - x_1\left(b_i^2 + b_i\frac{x_2)}{b_i^2+b_i}x_3 + x_4\right]\ ^2$ The coefficients are displayed in Appendix Table 12.	$[-5,5]^4$	0.0003075
$f_{16}(X) = 4x_1^2 - 2.1x_1^4 + \frac{1}{3}x_1^6 + x_1\ x_2 - 4x_2^2 + 4x_2^4$	$[-5,5]^2$	−1.0316285
$f_{17}(X) = \left(x_2 - \frac{5.1}{4\pi^2}x_1^2 + \frac{5}{\pi}x_1 - 6\right)\ ^2 + 10\left(1 - \frac{1}{8\pi}\right)\cos x_1 + 10$	$[-5,10]\times[0,15]$	0.398
$f_{18}(X) = [1 + (x_1 + x_2 + 1)\ ^2 \times (19 - 14x_1 + 3x_1^2 - 14x_2 + 6x_1\ x_2 + 3x_2^2)] \times$ $[30 + (2x_1 - 3x_2)\ ^2 \times (18 - 32x_1 + 12x_1^2 + 48x_2 - 36x_1\ x_2 + 27x_2^2)]$	$[-2,2]^2$	3
$f_{19}(X) = -\sum_{i=1}^{4} c_i \exp\left(-\sum_{j=1}^{3} a_{ij}\left(x_j - p_{ij}\right)\ ^2\right)$ The coefficients are displayed in Appendix Table 13.	$[0,1]^3$	−3.86
$f_{20}(X) = -\sum_{i=1}^{4} c_i \exp\left(-\sum_{j=1}^{6} a_{ij}\left(x_j - p_{ij}\right)\ ^2\right)$ The coefficients are displayed in Appendix Table 14.	$[0,1]^6$	−3.32
$f_{21}(X) = -\sum_{i=1}^{5}[(X - a_i)(X - a_i)\ ^T + c_i]^{-1}$ The coefficients are displayed in Appendix Table 15.	$[0,10]^4$	−10.1532
$f_{22}(X) = -\sum_{i=1}^{7}[(X - a_i)(X - a_i)\ ^T + c_i]^{-1}$ The coefficients are displayed in Appendix Table 15.	$[0,10]^4$	−10.4028
$f_{23}(X) = -\sum_{i=1}^{10}[(X - a_i)(X - a_i)\ ^T + c_i]^{-1}$ The coefficients are displayed in Appendix Table 15.	$[0,10]^4$	−10.5363

Table 12 Coefficients related to benchmark function f_{15}

i	a_i	b_i^{-1}
1	0.1957	0.25
2	0.1947	0.5
3	0.1735	1
4	0.1600	2
5	0.0844	4
6	0.0627	6
7	0.0456	8
8	0.0342	10
9	0.0323	12
10	0.0235	14
11	0.0246	16

Table 13 Coefficients related to benchmark function f_{19}

i	a_{i1}	a_{i2}	a_{i3}	c_i	p_{i1}	p_{i2}	p_{i3}
1	3	10	30	1	0.3689	0.1170	0.2673
2	0.1	10	35	2	0.4699	0.4387	0.7470
3	3	10	30	3	0.1091	0.8732	0.5547
4	0.1	10	35	4	0.03815	0.5743	0.8828

Table 14 Coefficients related to benchmark function f_{20}

i	a_{i1}	a_{i2}	a_{i3}	a_{i4}	a_{i5}	a_{i6}	c_i	p_{i1}	p_{i2}	p_{i3}	p_{i4}	p_{i5}	p_{i6}
1	10	3	17	3.5	1.7	8	1	0.1312	0.1696	0.5569	0.0124	0.8283	0.5886
2	0.05	10	17	0.1	8	14	1.2	0.2329	0.4135	0.8307	0.3736	0.1004	0.9991
3	3	3.5	1.7	10	17	8	3	0.2348	0.1415	0.3522	0.2883	0.3047	0.6650
4	17	8	0.05	10	0.1	14	3.2	0.4047	0.8828	0.8732	0.5743	0.1091	0.0381

Table 15 Coefficients related to benchmark function f_{21-23}

i	a_{i1}	a_{i2}	a_{i3}	a_{i4}	c_i
1	4	4	4	4	0.1
2	1	1	1	1	0.2
3	8	8	8	8	0.2
4	6	6	6	6	0.4
5	3	7	3	7	0.4
6	2	9	2	9	0.6
7	5	5	3	3	0.3
8	8	1	8	1	0.7
9	6	2	6	2	0.5
10	7	3.6	7	3.6	0.5

References

1. Agrawal S, Panda R, Bhuyan S, Panigrahi BK (2013) Tsallis entropy based optimal multilevel thresholding using cuckoo search algorithm. Swarm Evol Comput 11:16–30. https://doi.org/10.1016/j.swevo.2013.02.001
2. Agrawal S, Panda R, Abraham A (2018) A novel diagonal class entropy-based multilevel image Thresholding using coral reef optimization. IEEE Trans Syst man, Cybern Syst:1–9. https://doi.org/10.1109/TSMC.2018.2859429
3. Ahmadi M, Kazemi K, Aarabi A, Niknam T, Helfroush MS (2019) Image segmentation using multilevel thresholding based on modified bird mating optimization. Multimed Tools Appl 78:23003–23027. https://doi.org/10.1007/s11042-019-7515-6
4. Ayala HVH, dos Santos FM, Mariani VC, dos Coelho LS (2015) Image thresholding segmentation based on a novel beta differential evolution approach. Expert Syst Appl 42:2136–2142. https://doi.org/10.1016/j.eswa.2014.09.043
5. Baby Resma KP, Nair MS (2018) Multilevel thresholding for image segmentation using krill herd optimization algorithm. J King Saud Univ - Comput Inf Sci. https://doi.org/10.1016/j.jksuci.2018.04.007
6. Barthelemy P, Bertolotti J, Wiersma DS (2008) A levy flight for light. Nature 453:495–498
7. Bhandari A (2015) Tsallis entropy based multilevel Thresholding for colored satellite image segmentation using evolutionary algorithms. Expert Syst Appl 42:8707–8730. https://doi.org/10.1016/j.eswa.2015.07.025
8. Bhandari AK, Singh VK, Kumar A, Singh GK (2014) Cuckoo search algorithm and wind driven optimization based study of satellite image segmentation for multilevel thresholding using Kapur's entropy. Expert Syst Appl 41:3538–3560. https://doi.org/10.1016/j.eswa.2013.10.059
9. Chen Y, He F, Li H, Zhang D, Wu Y (2020) A full migration BBO algorithm with enhanced population quality bounds for multimodal biomedical image registration. Appl Soft Comput 93:106335. https://doi.org/10.1016/j.asoc.2020.106335

10. Dhiman G, Kaur A (2019) STOA: a bio-inspired based optimization algorithm for industrial engineering problems. Eng Appl Artif Intell 82:148–174. https://doi.org/10.1016/j.engappai.2019.03.021
11. Education H, Shahabi F, Pourahangarian F, Beheshti H (2019) A multilevel image thresholding approach based on crow search algorithm and Otsu method. J J Decis Oper Res 4:33–41. https://doi.org/10.22105/dmor.2019.88580
12. El Aziz MA, Ewees AA, Hassanien AE (2017) Whale optimization algorithm and moth-flame optimization for multilevel thresholding image segmentation. Expert Syst Appl 83:242–256. https://doi.org/10.1016/j.eswa.2017.04.023
13. Freixenet J, Muñoz X, Raba D et al (2002) Yet another survey on image segmentation: region and boundary information integration. Springer, Berlin Heidelberg, Berlin, Heidelberg, pp 408–422
14. Fu KS, Mui JK (1981) A survey on image segmentation. Pattern Recogn 13:3–16. https://doi.org/10.1016/0031-3203(81)90028-5
15. Gandomi AH, Yang X-S, Alavi AH (2011) Mixed variable structural optimization using firefly algorithm. Comput Struct 89:2325–2336. https://doi.org/10.1016/j.compstruc.2011.08.002
16. Gandomi A, Yang X-S, Alavi A (2013) Cuckoo search algorithm: a metaheuristic approach to solve structural optimization problems. Eng Comput 29:245. https://doi.org/10.1007/s00366-012-0308-4
17. Gao H, Xu W, Sun J, Tang Y (2010) Multilevel Thresholding for image segmentation through an improved quantum-behaved particle swarm algorithm. IEEE Trans Instrum Meas 59:934–946. https://doi.org/10.1109/TIM.2009.2030931
18. Hammouche K, Diaf M, Siarry P (2008) A multilevel automatic thresholding method based on a genetic algorithm for a fast image segmentation. Comput Vis Image Underst 109:163–175. https://doi.org/10.1016/j.cviu.2007.09.001
19. Heidari AA, Mirjalili S, Faris H, Aljarah I, Mafarja M, Chen H (2019) Harris hawks optimization: algorithm and applications. Futur Gener Comput Syst 97:849–872. https://doi.org/10.1016/j.future.2019.02.028
20. Horng MHM-H (2010) Multilevel minimum cross entropy threshold selection based on the honey bee mating optimization. Expert Syst Appl 37:4580–4592. https://doi.org/10.1016/j.eswa.2009.12.050
21. Horng MHM-H (2011) Multilevel thresholding selection based on the artificial bee colony algorithm for image segmentation. Expert Syst Appl 38:13785–13791. https://doi.org/10.1016/j.eswa.2011.04.180
22. Horng MHM-H, Liou RJR-J (2011) Multilevel minimum cross entropy threshold selection based on the firefly algorithm. Expert Syst Appl 38:14805–14811. https://doi.org/10.1016/j.eswa.2011.05.069
23. Jia H, Peng X, Song W et al (2019) Masi entropy for satellite color image segmentation using tournament-based Lévy multiverse optimization algorithm. Remote Sens 11:942. https://doi.org/10.3390/rs11080942
24. Kandhway P, Bhandari AK (2019) A water cycle algorithm-based multilevel Thresholding system for color image segmentation using Masi entropy. Circuits, Syst Signal Process 38:3058–3106. https://doi.org/10.1007/s00034-018-0993-3
25. Kapur JNN, Sahoo PKK, Wong AKCKC (1985) A new method for gray-level picture thresholding using the entropy of the histogram. Comput Vision, Graph Image Process 29:273–285. https://doi.org/10.1016/0734-189X(85)90125-2
26. Khairuzzaman AKM, Chaudhury S (2017) Multilevel thresholding using grey wolf optimizer for image segmentation. Expert Syst Appl 86:64–76. https://doi.org/10.1016/j.eswa.2017.04.029
27. Khairuzzaman AK, Chaudhury S (2019) Masi entropy based multilevel thresholding for image segmentation. Multimed Tools Appl 78:33573–33591. https://doi.org/10.1007/s11042-019-08117-8
28. Li H, He F, Liang Y, Quan Q (2020) A dividing-based many-objective evolutionary algorithm for large-scale feature selection. Soft Comput 24:6851–6870. https://doi.org/10.1007/s00500-019-04324-5
29. Li H, He F, Chen Y, Luo J (2020) Multi-objective self-organizing optimization for constrained sparse array synthesis. Swarm Evol Comput 58:100743. https://doi.org/10.1016/j.swevo.2020.100743
30. Li H, He F, Chen Y (2020) Learning dynamic simultaneous clustering and classification via automatic differential evolution and firework algorithm. Appl Soft Comput 96:106593. https://doi.org/10.1016/j.asoc.2020.106593
31. Liang Y, He F, Zeng X (2020) 3D mesh simplification with feature preservation based on whale optimization algorithm and differential evolution. Integr Comput Aided Eng 27:417–435. https://doi.org/10.3233/ICA-200641
32. Liao P-S, Chen T-S, Chung P-C (2001) A fast algorithm for multilevel Thresholding. J Inf Sci Eng 17:713–727
33. Liu J, Li W, Tian Y (1991) Automatic thresholding of gray-level pictures using two-dimension Otsu method. In: China., 1991 international conference on circuits and systems, vol 1, pp 325–327
34. Martin D, Fowlkes C, Tal D, Malik J (2001) A database of human segmented natural images and its application to evaluating segmentation algorithms and measuring ecological statistics. In: Proceedings eighth IEEE international conference on computer vision, ICCV 2001, vol 2, pp 416–423

35. Masi M (2005) A step beyond Tsallis and Renyi entropies. Phys Lett A 338:217–224. https://doi.org/10.1016/j.physleta.2005.01.094
36. Mirjalili S (2015) Moth-flame optimization algorithm: a novel nature-inspired heuristic paradigm. Knowledge-Based Syst 89:228–249. https://doi.org/10.1016/j.knosys.2015.07.006
37. Mirjalili S, Mirjalili SM, Lewis A (2014) Grey wolf optimizer. Adv Eng Softw 69:46–61. https://doi.org/10.1016/j.advengsoft.2013.12.007
38. Mlakar U, Potočnik B, Brest J (2016) A hybrid differential evolution for optimal multilevel image thresholding. Expert Syst Appl 65:221–232. https://doi.org/10.1016/j.eswa.2016.08.046
39. Naik MK, Panda R (2016) A novel adaptive cuckoo search algorithm for intrinsic discriminant analysis based face recognition. Appl Soft Comput 38:661–675. https://doi.org/10.1016/j.asoc.2015.10.039
40. Naik MK, Samantaray L, Panda R (2016) A hybrid CS–GSA algorithm for optimization. In: Hybrid soft computing approaches: research and applications, pp 3–35
41. Naik MK, Wunnava A, Jena B, Panda R (2020) 1. Nature-inspired optimization algorithm and benchmark functions: a literature survey. In: Bisht DCS, Ram M (eds) Computational Intelligence, 3rd edn. De Gruyter, Berlin, Boston, pp 1–26
42. Nie F, Zhang P, Li J, Ding D (2017) A novel generalized entropy and its application in image thresholding. Signal Process 134:23–34. https://doi.org/10.1016/j.sigpro.2016.11.004
43. Otsu (1979) Otsu_1979_otsu_method. IEEE Trans Syst Man Cybern C:62–66. https://doi.org/10.1109/TSMC.1979.4310076
44. Pal NR, Pal SK (1989) Entropic thresholding. Signal Process 16:97–108. https://doi.org/10.1016/0165-1684(89)90090-X
45. Pal NR, Pal SK (1993) A review on image segmentation techniques. Pattern Recogn 26:1277–1294. https://doi.org/10.1016/0031-3203(93)90135-J
46. Panda R, Agrawal S, Bhuyan S (2013) Edge magnitude based multilevel thresholding using cuckoo search technique. Expert Syst Appl 40:7617–7628. https://doi.org/10.1016/j.eswa.2013.07.060
47. Panda R, Agrawal S, Samantaray L, Abraham A (2017) An evolutionary gray gradient algorithm for multilevel thresholding of brain MR images using soft computing techniques. Appl Soft Comput 50:94–108. https://doi.org/10.1016/j.asoc.2016.11.011
48. Pavesic N, Ribaric S (2000) Gray level thresholding using the Havrda and Charvat entropy. In: 2000 10th Mediterranean Electrotechnical conference. Information technology and Electrotechnology for the Mediterranean countries. Proceed MeleCon (cat. No.00CH37099) 2:631–634
49. Peng-Yeng Y, Ling-Hwei C (1994) A new method for multilevel thresholding using symmetry and duality of the histogram. In: proceedings of ICSIPNN '94. International Conference on Speech, Image Processing and Neural Networks. Pp 45–48 vol.1
50. Portes de Albuquerque M, Esquef IA, Gesualdi Mello AR, Portes de Albuquerque M (2004) Image thresholding using Tsallis entropy. Pattern Recogn Lett 25:1059–1065. https://doi.org/10.1016/j.patrec.2004.03.003
51. Rao RV, Patel V (2013) An improved teaching-learning-based optimization algorithm for solving unconstrained optimization problems. Sci Iran 20:710–720. https://doi.org/10.1016/j.scient.2012.12.005
52. Renyi A (1961) On measures of entropy and information. In: Proceedings of the fourth Berkeley symposium on mathematical statistics and probability, volume 1: contributions to the theory of statistics. University of California Press, Berkeley, Calif, pp 547–561
53. Sahoo PK, Arora G (2004) A thresholding method based on two-dimensional Renyi's entropy. Pattern Recogn 37:1149–1161. https://doi.org/10.1016/j.patcog.2003.10.008
54. Sahoo PK, Arora G (2006) Image thresholding using two-dimensional Tsallis–Havrda–Charvát entropy. Pattern Recogn Lett 27:520–528. https://doi.org/10.1016/j.patrec.2005.09.017
55. Sahoo PK, Soltani S, Wong AKC (1988) A survey of thresholding techniques. Comput Vision, Graph Image Process 41:233–260. https://doi.org/10.1016/0734-189X(88)90022-9
56. Sankur B, Sezgin M (2001) Image thresholding techniques: a survey over categories. Pattern Recogn 34:1573–1583
57. Sarkar S, Das S (2013) Multilevel image Thresholding based on 2D histogram and maximum Tsallis entropy— a differential evolution approach. IEEE Trans Image Process 22:4788–4797. https://doi.org/10.1109/TIP.2013.2277832
58. Sathya PD, Kayalvizhi R (2011) Modified bacterial foraging algorithm based multilevel thresholding for image segmentation. Eng Appl Artif Intell 24:595–615. https://doi.org/10.1016/j.engappai.2010.12.001
59. Sezgin M, Sankur B (2004) Survey over image thresholding techniques and quantitative performance evaluation. J Electron Imaging 13:146–168. https://doi.org/10.1117/1.1631315
60. Shubham S, Bhandari AK (2019) A generalized Masi entropy based efficient multilevel thresholding method for color image segmentation. Multimed Tools Appl 78:17197–17238. https://doi.org/10.1007/s11042-018-7034-x

61. Simon D (2009) Biogeography-based optimization. Evol Comput IEEE Trans 12:702–713. https://doi.org/10.1109/TEVC.2008.919004
62. Song JH, Cong W, Li JJ (2017) A fuzzy C-means clustering algorithm for image segmentation using nonlinear weighted local information. J Inf Hiding Multimed Signal Process 8:578–588
63. Sri Madhava Raja N, Rajinikanth V, Latha K (2014) Otsu based optimal multilevel image Thresholding using firefly algorithm. J Model Simul Eng 2014:17–17. https://doi.org/10.1155/2014/794574
64. Tsallis C (1988) Possible generalization of Boltzmann-Gibbs statistics. J Stat Phys 52:479–487. https://doi.org/10.1007/BF01016429
65. Tsallis C (2001) Nonextensive statistical mechanics and its applications. Lect Notes Phys 560:3–98
66. Upadhyay P, Chhabra JK (2019) Kapur's entropy based optimal multilevel image segmentation using. Crow Search Algorithm Appl Soft Comput:105522. https://doi.org/10.1016/j.asoc.2019.105522
67. Xing Z, Jia H (2020) Modified thermal exchange optimization based multilevel thresholding for color image segmentation. Multimed Tools Appl 79:1137–1168. https://doi.org/10.1007/s11042-019-08229-1
68. Yang X-S (2010) Nature-inspired Metaheuristic algorithms
69. Yang X-S (2012) Flower pollination algorithm for global optimization. In: Durand-Lose J, Jonoska N (eds) Unconventional computation and natural computation: 11th international conference, UCNC 2012, Orléan, France, September 3–7, 2012. Proceedings. Springer Berlin Heidelberg, Berlin, Heidelberg, pp 240–249
70. Yang X-S, Gandomi A (2012) Bat algorithm: a novel approach for global engineering optimization. Eng Comput 29:464–483. https://doi.org/10.1108/02644401211235834
71. Yao X, Yong L, Guangming L (1999) Evolutionary programming made faster. Evol Comput IEEE Trans 3: 82–102. https://doi.org/10.1109/4235.771163
72. Yin P-Y (2007) Multilevel minimum cross entropy threshold selection based on particle swarm optimization. Appl Math Comput 184:503–513. https://doi.org/10.1016/j.amc.2006.06.057
73. Yin P-Y, Chen L-H (1997) A fast iterative scheme for multilevel thresholding methods. Signal Process 60: 305–313. https://doi.org/10.1016/S0165-1684(97)00080-7
74. Zaitoun NM, Aqel MJ (2015) Survey on image segmentation techniques. Procedia Comput Sci 65:797–806. https://doi.org/10.1016/j.procs.2015.09.027
75. Zhang Y, Wu L (2011) Optimal Multi-Level Thresholding Based on Maximum Tsallis Entropy via an Artificial Bee Colony Approach 13:841–859
76. Zhang H, Fritts JE, Goldman SA (2008) Image segmentation evaluation: a survey of unsupervised methods. Comput Vis Image Underst 110:260–280. https://doi.org/10.1016/j.cviu.2007.08.003
77. Zhang L, Zhang L, Mou X et al (2011) FSIM: a feature similarity index for image quality assessment. IEEE Trans Image Process 20:2378–2386. https://doi.org/10.1109/TIP.2011.2109730
78. Zhiwei Y, Zhaobao Z, Xin Y, Xiaogang N (2005) Automatic threshold selection based on ant colony optimization algorithm. In: 2005 international conference on neural networks and brain, pp 728–732
79. Zhou W, Bovik AC, Sheikh HR, Simoncelli EP (2004) Image quality assessment: from error visibility to structural similarity. IEEE Trans Image Process 13:600–612. https://doi.org/10.1109/TIP.2003.819861

Affiliations

Manoj Kumar Naik [1] • Rutuparna Panda [2] • Aneesh Wunnava [1] • Bibekananda Jena [3] • Ajith Abraham [4]

Rutuparna Panda
r_ppanda@yahoo.co.in

Aneesh Wunnava
aneeshwunnava@gmail.com

Bibekananda Jena
bibekananda.jena@gmail.com

Ajith Abraham
ajith.abraham@ieee.org

[1] Faculty of Engineering and Technology, Siksha O Anusandhan, Bhubaneswar, Odisha 751030, India

[2] Dept. of Electronics and Telecommunication Engineering, Veer Surendra Sai University of Technology, Burla, Odisha 768018, India

[3] Dept. of Electronics and Communication Engineering, Anil Neerukonda Institute of Technology & Science, Sangivalasa, Visakhapatnam, Andhra Pradesh 531162, India

[4] Machine Intelligence Research Labs, Scientific Network for Innovation and Research Excellence, Washington 98071-2259, USA